Aalto University
School of Science
Degree Programme in Engineering Physics and Mathematics

Tuomas Ollikainen

Two-qubit gates in a microwave photonic quantum computer

Master's thesis
Espoo, 01.07.2015

Supervisor: Prof. Matti Kaivola
Advisor: Dr. Mikko Möttönen

Aalto University
School of Science
Degree Programme in Engineering Physics and Mathematics

ABSTRACT OF
MASTER'S THESIS

Author: Tuomas Ollikainen

Title:
Two-qubit gates in a microwave photonic quantum computer

Date: 01.07.2015 **Pages:** 6 + 68

Major: Engineering Physics **Code:** Tfy-125

Supervisor: Prof. Matti Kaivola

Advisor: Dr. Mikko Möttönen

Building a scalable quantum computer is one of the greatest challenges of this century. A quantum computer should be able to execute quantum algorithms which promise great speed up in solving certain computational problems.

Microwave photons in superconducting circuits offer a promising platform for quantum computing due to their long coherence times, and the ease of their generation and control. Single-qubit quantum gates are implemented with conventional microwave components. However, implementing entangling two-qubit gates for photonic qubits is considerably difficult because photons do not interact with each other naturally.

In this thesis, we investigate the effective interactions between photons mediated by superconducting qubits. Especially, the nonlinear effects in the photonic states generated by these interactions are studied.

Based on the analysis of the scattering properties of the system, we present a design for a nonlinear phase shifter device, which yields a photon-number-dependent phase shift in the transmitted photons. Furthermore, we show how entangling two-qubit gates can be implemented using the presented nonlinear phase shifter.

Keywords: quantum computing, quantum gates, microwave photon, superconducting transmission line, nonlinear phase shifter

Language: English

Aalto-yliopisto
Perustieteiden korkeakoulu
Teknillisen fysiikan ja matematiikan koulutusohjelma

DIPLOMITYÖN
TIIVISTELMÄ

Tekijä:	Tuomas Ollikainen		
Työn nimi:	Kaksikubittiportit mikroaaltofotonisessa kvanttitietokoneessa		
Päiväys:	01.07.2015	**Sivumäärä:**	6 + 68
Pääaine:	Teknillinen fysiikka	**Koodi:**	Tfy-125
Valvoja:	prof. Matti Kaivola		
Ohjaaja:	dos. Mikko Möttönen		

Yksi vuosisatamme suurimmista haasteista on skaalautuvan kvanttitietokoneen rakentaminen. Kvanttitietokoneen tulisi pystyä suorittamaan kvanttialgoritmeja, jotka mahdollistavat tietyille laskennallisille ongelmille klassisia vastineita huomattavasti nopeamman ratkaisemisen.

Mikroaaltofotonit suprajohtavissa piireissä tarjoavat lupaavan alustan kvanttilaskennalle niiden suhteellisen pitkien koherenssiaikojen sekä niiden luomisen ja muokkaamisen helppouden vuoksi. Yksikubittiportteja on mahdollista toteuttaa käyttäen tavanomaisia mikroaaltokomponentteja. Lomittavien kaksikubittiporttien toteuttaminen on kuitenkin erityisen haastavaa, sillä fotonit eivät vuorovaikuta keskenään luonnollisesti.

Tässä työssä tutkimme mikroaaltofotonien kokemaa efektiivistä vuorovaikutusta, jonka välittäjänä toimivat suprajohtavat kubitit. Tutkimme erityisesti näiden vuorovaikutusten tuottamia epälineaarisia vaikutuksia fotonisissa tiloissa.

Perustuen tällaisen systeemin sirontaominaisuuksiin, esittelemme mallin epälineaariselle vaiheensiirtimelle, joka tuottaa fotonien lukumäärästä riippuvan vaiheensiirron systeemin läpäiseville fotoneille. Lisäksi näytämme kuinka tietyt lomittavat kaksikubittiportit voidaan toteuttaa käyttämällä esiteltyä epälineaarista vaiheensiirrintä.

Asiasanat:	kvanttilaskenta, kvanttiportit, mikroaaltofotoni, suprajohtava siirtolinja, epälineaarinen vaiheensiirrin
Kieli:	englanti

Acknowledgements

This thesis was written in the Quantum Computing and Devices (QCD) research group in the Department of Applied Physics of Aalto University School of Science. I thank the current Head of Department, Prof. Matti Kaivola, for supervising this thesis. I also thank the leader of the QCD group, Dr. Mikko Möttönen, for instructing this thesis, and also for the guidance he has given me throughout the time I have worked in his group. I also thank all other members of the QCD group for creating an inspiring working environment.

I also wish to show my gratitude to my classmates at Aalto University, as well as to the friends outside the university. Finally, I am grateful to my family for being loving and supportive.

Espoo, 01.07.2015

Tuomas Ollikainen

Contents

Acknowledgements **iv**

Contents **v**

1 Introduction **1**

2 Background **3**
2.1 Quantum computing 3
2.1.1 Single- and multi-qubit states 3
2.1.2 Quantum entanglement 4
2.1.3 Single-qubit gates 5
2.1.4 Multi-qubit gates 6
2.2 Quantum computing with microwave photons 7
2.2.1 Dual-rail representation 8
2.2.2 Quantum gates 8
2.2.3 Hong–Ou–Mandel effect 10
2.3 Superconducting qubits 11
2.3.1 Superconductivity 11
2.3.2 Josephson junction 11
2.3.3 Cooper pair box 12
2.3.4 Transmon 12
2.4 Quantum optics 13
2.4.1 Jaynes–Cummings model 13
2.4.2 Dispersive limit 14
2.4.3 Input-output theory 15

3 Methods: waveguide quantum electrodynamics **16**
3.1 Distributed-element model 16
3.2 Continuum limit 19
3.3 Quantization 20
3.3.1 Transmission line 20

3.3.2 Superconducting qubit 24
3.3.3 Transmon regime 26
3.3.4 Coupling term 26
3.4 Real-space Hamiltonian 27

4 Methods: few-photon scattering **31**
4.1 Single-photon scattering 31
4.1.1 Scattering from a single qubit 31
4.1.2 Scattering from three qubits 32
4.2 Two-photon scattering 34
4.2.1 Two-photon eigenstate in the position basis 41
4.2.2 Markovian approximation 42
4.2.3 Summary of the Green's function method 43

5 Results **45**
5.1 Nonlinear phase shifter 45
5.1.1 Single-photon transmission 47
5.1.2 Two-photon transmission 48
5.1.3 Two-photon reflection 49
5.1.4 Spatial correlations 50
5.1.5 Response of the device 53
5.1.6 Error sources 54
5.2 Two-qubit gates 55
5.2.1 Conditional-phase-shift gate 55
5.2.2 Controlled-Z gate 57
5.2.3 Gate fidelities 57

6 Conclusions **61**

References **63**

A Single-photon scattering coefficients **66**

B Nonlinear corrections **68**

Chapter 1

Introduction

The paradigm of quantum computing emerged in the 1980s [1, 2] and the field has been under extensive study since, both theoretically and experimentally. The operation of a quantum computer is based on the manipulation of quantum bits, qubits, by taking advantage of the quantum degrees of freedom in the computation process. A quantum computer executes quantum algorithms, which promise great speed up in solving certain computational tasks over their classical counterparts. Two well-known examples where the use of quantum algorithms offer such a quantum speed up are integer factorization [3] and searching for data from an unsorted database [4].

Building a scalable quantum computer still remains one of the major challenges in modern physics. Several candidates for the physical system representing the qubit have been proposed including, but not limited to, trapped ions [5], spin-1/2 nuclei [6, 7], and quantum dots [8]. One alternative scheme is to use photons to carry quantum information [9]. Photons exhibit long coherence times and they are relatively simple to generate and control. Single-qubit gates can be implemented using conventional linear optical or microwave components, such as phase shifters and beam splitters.

For universal quantum computing, one should be able to realize quantum gates that create entanglement between two qubits. Implementing these two-qubit gates is difficult with photons due to the limited interactions between them. Entanglement can, in principle, be created between photons with the help of the nonlinear Kerr medium. However, the nonlinear effect of such a medium is effectively negligible and some percentage of photons is always absorbed in the medium, rendering two-qubit gates difficult to realize with purely optical means.

Superconducting circuits offer another promising platform for quantum computing [10]. This emerging field is generally referred to as circuit quantum electrodynamics. Quantum devices in these circuits are typically based

on Josephson junctions which are used to create effective two-level systems that display their quantum properties in electric quantities, such as current and voltage. These two-level systems, referred to as superconducting qubits, interact strongly with spatially confined microwave fields. The strong coupling between the superconducting qubits and microwave photons may offer an alternative way to create Kerr-like interactions and entanglement between photons [11, 12].

In this thesis, we study microwave photons propagating in a superconducting transmission line. We treat the transmission line quantum mechanically and investigate the linear as well as the nonlinear scattering properties for single- and two-photon input states with one or several superconducting qubits coupled to the transmission line. Moreover, we show how these properties can be utilized in the creation of entangling two-qubit quantum gates in a microwave photonic quantum computer.

This thesis is structured as follows: In Ch. 2, we review the relevant theoretical background related to this thesis. These include the theories of quantum computing, photonic quantum computing, superconducting qubits, and quantum optics. In Ch. 3, we derive the quantum-mechanical Hamiltonian for the superconducting transmission line to which an arbitrary number of superconducting qubits are capacitively coupled. In Ch. 4, we present the methods for calculating the scattering properties of the system, with one or two photons propagating in the circuit. These methods are then used in Ch. 5, where we present a design for a nonlinear phase shifter device based on a system with three superconducting qubits coupled to the transmission line. The possible error sources are also analyzed. Furthermore, we show how this nonlinear phase shifter could be used as a component in entangling two-qubit quantum gates in a microwave photonic quantum computer. Finally, in Ch. 6, we draw conclusions on the main results of this thesis and discuss the possible future research on the topic.

Chapter 2

Background

In this chapter, we present the theoretical foundations for quantum computing, photonic quantum computing, and superconductivity. We also discuss different realizations of superconducting qubits. Finally, we provide a short introduction to quantum optics and input-output theory.

2.1 Quantum computing

2.1.1 Single- and multi-qubit states

A physical quantum bit, or a qubit, is a quantum-mechanical system with two accessible states. It is a quantum analogue of a bit used in classical computing, in which a single classical bit is strictly in one of the two states, 0 or 1. The quantum-mechanical basis states of a qubit are written as states $|0\rangle$ and $|1\rangle$, corresponding to their counterparts in classical computing. In addition to exactly being in one of these two basis states, a qubit is also allowed to be in a superposition. Hence, the general state of a single-qubit system $|\psi\rangle$ is written as

$$|\psi\rangle = \alpha\,|0\rangle + \beta\,|1\rangle\,, \tag{2.1}$$

where the coefficients α and β are complex numbers and the states $|0\rangle$ and $|1\rangle$ form an orthonormal basis. The state vector $|\psi\rangle$ is normalized, giving rise to a restriction that $|\alpha|^2 + |\beta|^2 = 1$. The physical interpretation of the coefficients is that $|\alpha|^2$ and $|\beta|^2$ are the probabilities of finding the qubit in the states $|0\rangle$ and $|1\rangle$, respectively.

Since the norm of a qubit state always equals to unity, the state can be uniquely represented with a vector on the unit sphere. The unit sphere in this context is generally referred to as the Bloch sphere. In this representation,

the general state of the qubit in Eq. (2.1) can be rewritten as

$$|\psi\rangle = \cos\left(\frac{\theta}{2}\right)|0\rangle + e^{i\varphi}\sin\left(\frac{\theta}{2}\right)|1\rangle\,, \tag{2.2}$$

where $\theta \in [0,\pi]$ is the polar angle and $\varphi \in [0,2\pi)$ is the azimuthal angle in spherical coordinates. Mathematically, there should be a global phase factor $e^{i\gamma}$ multiplying both terms in Eq. (2.2), but since it has no observable effects on the qubit, it is not included [13].

The state of a system with n distinct qubits can be expressed as

$$|\Psi\rangle = \sum_{i_1=0}^{1}\sum_{i_2=0}^{1}...\sum_{i_n=0}^{1}\alpha_{i_1,i_2,...,i_n}|i_1 i_2 ... i_n\rangle\,, \tag{2.3}$$

where $|i_1 i_2 ... i_n\rangle = |i_1\rangle|i_2\rangle ... |i_n\rangle = |i_1\rangle \otimes |i_2\rangle \otimes ... \otimes |i_n\rangle$ is a shorthand notation for the tensor product of the n-qubit basis vectors, spanning the 2^n dimensional complex Hilbert space. The coefficients $\alpha_{i_1,i_2,...,i_n}$ are normalized such that $\sum_{i_1=0}^{1}\sum_{i_2=0}^{1}...\sum_{i_n=0}^{1}|\alpha_{i_1,i_2,...,i_n}|^2 = 1$.

As an instructive example, we consider a system of two qubits. The basis is given by $\{|00\rangle, |01\rangle, |10\rangle, |11\rangle\}$, where the first digit in the state vector denotes the state of the first qubit and the second digit denotes the state of the second qubit. Suppose that the qubit is initially in a superposition

$$\left|\psi^{(2)}\right\rangle = \alpha_{00}|00\rangle + \alpha_{01}|01\rangle + \alpha_{10}|10\rangle + \alpha_{11}|11\rangle\,, \tag{2.4}$$

where $|\alpha_{00}|^2 + |\alpha_{01}|^2 + |\alpha_{10}|^2 + |\alpha_{11}|^2 = 1$. We then measure the state of the second qubit and find it in state $|1\rangle$. After the measurement, according to the quantum measurement postulate, the final state is given by

$$\left|\tilde{\psi}^{(2)}\right\rangle = \frac{1}{\sqrt{|\alpha_{01}|^2 + |\alpha_{11}|^2}}\left(\alpha_{01}|01\rangle + \alpha_{11}|11\rangle\right), \tag{2.5}$$

where the state of the second qubit is fixed at $|1\rangle$ and the first qubit is still in a superposition of its basis states.

2.1.2 Quantum entanglement

In addition to the superposition principle, another important phenomenon that quantum computing makes use of is quantum entanglement. A quantum state is defined as entangled, if it is not separable. The n-qubit state is separable, if it can be written as a direct product of single-qubit states as

$$\left|\psi^{(n)}\right\rangle = |\psi_1\rangle \otimes |\psi_2\rangle \otimes ... \otimes |\psi_n\rangle\,, \tag{2.6}$$

where $|\psi_i\rangle = \alpha_i |0\rangle + \beta_i |1\rangle$ is the ith single-qubit state. For example, if the two-qubit state from Eq. (2.4) is separable, we have

$$\begin{aligned} \left|\psi^{(2)}\right\rangle &= \alpha_{00} |00\rangle + \alpha_{01} |01\rangle + \alpha_{10} |10\rangle + \alpha_{11} |11\rangle \\ &= (\beta_0 |0\rangle + \beta_1 |1\rangle) \otimes (\beta'_0 |0\rangle + \beta'_1 |1\rangle) \\ &= |\psi_1\rangle \otimes |\psi_2\rangle , \end{aligned} \tag{2.7}$$

and hence $\beta_0\beta'_0 = \alpha_{00}$, $\beta_0\beta'_1 = \alpha_{01}$, $\beta_1\beta'_0 = \alpha_{10}$, and $\beta_1\beta'_1 = \alpha_{11}$. In fact, this condition defines the general form of a separable two-qubit state. An example of a non-separable, i.e., entangled, two-qubit state is given by

$$\left|\psi_{\mathrm{e}}^{(2)}\right\rangle = \frac{1}{\sqrt{2}} (|01\rangle + |10\rangle) . \tag{2.8}$$

There are no solutions for β_0, β'_0, β_1, and β'_1 that can satisfy the constraints that $\alpha_{01} = \alpha_{10} = 1/\sqrt{2}$ and $\alpha_{00} = \alpha_{11} = 0$, given the general separable two-qubit state of Eq. (2.7). Hence, the state in Eq. (2.8) is an entangled state.

2.1.3 Single-qubit gates

Quantum information, represented by qubits, is manipulated with quantum algorithms. These algorithms consist of quantum gates which can non-trivially act on single- or multi-qubit states. A convenient way to represent the operation of quantum gates is with the use of linear algebra. First, we represent the general single-qubit state in the vector notation with the basis vectors corresponding to states $|0\rangle$ and $|1\rangle$ as

$$|\psi\rangle = \alpha |0\rangle + \beta |1\rangle \;\widehat{=}\; \begin{pmatrix} \alpha \\ \beta \end{pmatrix} , \tag{2.9}$$

where the symbol '$\widehat{=}$' denotes the correspondence between the quantum state and the complex vector. Quantum gates are then expressed as 2×2 matrices that operate on the vector representing the quantum state. Since the norm of the quantum state must be conserved, the gate matrices need to be unitary. An example of a quantum gate that is equivalent to the classical NOT gate, which is a mapping $0 \to 1$ and $1 \to 0$, is given by the matrix

$$X = \begin{pmatrix} 0 & 1 \\ 1 & 0 \end{pmatrix} . \tag{2.10}$$

The gate is here referred to as X, since it has the same form as the Pauli spin matrix X, which corresponds to a rotation of π radians about the x-axis in the Bloch sphere.

Next, we aim to construct an arbitrary single-qubit gate. For this purpose, we introduce two important single-qubit gates: the Hadamard gate H

$$H = \frac{1}{\sqrt{2}} \begin{pmatrix} 1 & 1 \\ 1 & -1 \end{pmatrix}, \tag{2.11}$$

and the gate corresponding to rotation by an angle ϕ about z-axis in the Bloch sphere, given by

$$R_z(\phi) = e^{-iZ\phi/2} = \begin{pmatrix} e^{-i\phi/2} & 0 \\ 0 & e^{i\phi/2} \end{pmatrix}, \tag{2.12}$$

where Z is the Pauli spin matrix

$$Z = \begin{pmatrix} 1 & 0 \\ 0 & -1 \end{pmatrix}. \tag{2.13}$$

Thus, a general 2×2 unitary matrix U, which in the quantum computing scheme corresponds to an arbitrary single-qubit gate, can be expressed and decomposed with help of these gates as

$$\begin{aligned} U &= e^{i\varphi_1} \begin{pmatrix} \cos\theta & \sin\theta e^{i\varphi_2} \\ -\sin\theta e^{i\varphi_3} & \cos\theta e^{i(\varphi_2+\varphi_3)} \end{pmatrix} \\ &= e^{i(\varphi_1+\frac{\varphi_2}{2}+\frac{\varphi_3}{2})} R_z\left(\varphi_3 - \frac{\pi}{2}\right) H R_z(2\theta) H R_z\left(\varphi_2 + \frac{\pi}{2}\right). \end{aligned} \tag{2.14}$$

2.1.4 Multi-qubit gates

In the vector notation, multi-qubit states are represented as tensor products of single-qubit vectors. As an example, the general two-qubit state of Eq. (2.4) is written in the vector notation as

$$\left|\psi^{(2)}\right\rangle = \alpha_{00}\left|00\right\rangle + \alpha_{01}\left|01\right\rangle + \alpha_{10}\left|10\right\rangle + \alpha_{11}\left|11\right\rangle \;\widehat{=}\; \begin{pmatrix} \alpha_{00} \\ \alpha_{01} \\ \alpha_{10} \\ \alpha_{11} \end{pmatrix}. \tag{2.15}$$

Multi-qubit gates that operate independently on the single-qubit states are written as tensor products of the single-qubit gate matrices. However, interesting subset of multi-qubit gates are those that create entanglement between the qubits. One such gate is the controlled-NOT (CNOT) gate, that negates the state of the second qubit if the first qubit is in state $|1\rangle$. In the matrix

form, the CNOT gate is written as

$$\mathrm{CNOT} = \begin{pmatrix} 1 & 0 & 0 & 0 \\ 0 & 1 & 0 & 0 \\ 0 & 0 & 0 & 1 \\ 0 & 0 & 1 & 0 \end{pmatrix}. \tag{2.16}$$

To show explicitly how this gate can create entanglement, let us consider a two-qubit state in which the first qubit is in a superposition state $|\psi_1\rangle = 1/\sqrt{2}\,(|0\rangle + |1\rangle)$ and the second qubit is in state $|\psi_2\rangle = |0\rangle$. Operating with the CNOT gate maps the initially separable two-qubit state as $|\psi_1\rangle \otimes |\psi_2\rangle = 1/\sqrt{2}\,(|0\rangle + |1\rangle)\,|0\rangle \rightarrow 1/\sqrt{2}\,(|00\rangle + |11\rangle)$, which is an entangled state.

For the later chapters of this thesis, it is purposeful to present another two-qubit gate, the controlled-Z (CZ) gate. The CZ gate operates by only flipping the sign of the basis state $|11\rangle$. In the matrix notation, the operation is expressed as a matrix

$$\mathrm{CZ} = \begin{pmatrix} 1 & 0 & 0 & 0 \\ 0 & 1 & 0 & 0 \\ 0 & 0 & 1 & 0 \\ 0 & 0 & 0 & -1 \end{pmatrix}. \tag{2.17}$$

The two-qubit CNOT gate can be implemented with two Hadamard gate operations on the second qubit and a single CZ gate operation on both qubits, as

$$\mathrm{CNOT} = (I \otimes H)\,\mathrm{CZ}\,(I \otimes H)\,. \tag{2.18}$$

The quantum gates operating on the n-qubit states are presented as $2^n \times 2^n$ unitary matrices. It turns out that single-qubit gates together with a two-qubit CNOT gate form a universal set of n-qubit gates [14], i.e., an arbitrary n-qubit gate can be implemented with these gates.

2.2 Quantum computing with microwave photons

Physical realization of a quantum computer has proven to be a challenging task. In quantum computing, one has to be able to prepare and measure the qubits, and they should retain their quantum coherence for long enough such that quantum gate operations can be applied to them. In this thesis, we are using microwave photons as qubits. They have long coherence times and single-qubit gates can be conveniently implemented with phase shifters

and beam splitters, as we will show in Sec. 2.2.2. However, since photons do not naturally interact with each other, implementing entangling two-qubit gates is difficult.

2.2.1 Dual-rail representation

Photons have a polarization degree of freedom that could be used as the computational basis for the qubit. Instead, here we assume that the polarization direction is fixed and hence cannot be used as the basis for the qubit. This is the case, for example, with microwave photons in coplanar waveguides which are frequently used as waveguides in superconducting transmission lines.

We consider a photon with frequency ω and two physically separated waveguides. The quantum states in the two waveguides are defined as Fock states $|n_0\rangle = (\hat{a}_0^\dagger)^{n_0}/\sqrt{n_0!}\,|0\rangle$ and $|n_1\rangle = (\hat{a}_1^\dagger)^{n_1}/\sqrt{n_1!}\,|0\rangle$, corresponding to n_0 photons in the first waveguide and n_1 photons in the second waveguide. The operators $\hat{a}_i^\dagger$ and $\hat{a}_i$ are the creation and annihilation operators for a photon with frequency ω in the ith waveguide. In this system, we define the basis states of the qubit, $|0_\mathrm{Q}\rangle$ and $|1_\mathrm{Q}\rangle$, with a single photon propagating in one of the two waveguides, such that

$$|0_\mathrm{Q}\rangle \equiv |n_0 = 1\rangle \otimes |n_1 = 0\rangle \tag{2.19}$$

$$|1_\mathrm{Q}\rangle \equiv |n_0 = 0\rangle \otimes |n_1 = 1\rangle\,. \tag{2.20}$$

These states are eigenstates of the Hamiltonian describing the system

$$\hat{\mathcal{H}} = \hbar\omega \left(\hat{a}_0^\dagger \hat{a}_0 + \hat{a}_1^\dagger \hat{a}_1\right), \tag{2.21}$$

with eigenvalues $E_{n_0,n_1} = \hbar\omega(n_0 + n_1)$. We have omitted the constant zero-point energy shift from the Hamiltonian (2.21). The dual-rail representation is convenient, since the general single-qubit state, $\left|\psi^{(1)}\right\rangle = c_0\,|0_\mathrm{Q}\rangle + c_1\,|1_\mathrm{Q}\rangle$, changes only by an overall phase during time evolution, $\left|\psi^{(1)}(t)\right\rangle = e^{-i\omega t}\left|\psi^{(1)}\right\rangle$. Furthermore, the single-qubit operations preserve the number of photons in the system.

2.2.2 Quantum gates

The constant phase shifter in the dual-rail representation can be implemented by retarding one of the two modes with respect to the other. This can be carried out, for example, by adding to the first waveguide a material of length L with a refractive index differing from the bare waveguide by Δn. According to the classical electromagnetic theory, after passing through the

first waveguide, photons acquire a phase shift $(n+\Delta n)\omega L/c$, whereas photons traveling in the second waveguide without the retarding material acquire a shift $n\omega L/c$, where ω is the frequency of the photon and c is the speed of light in the vacuum. Hence, the phase difference between the photons traveling in the two waveguides is given by $\phi = \Delta n\omega L/c$. Assuming that the retarding material is applied to the waveguide corresponding to the $|1_{\mathrm{Q}}\rangle$ state, the basis states transform as $|0_{\mathrm{Q}}\rangle \to e^{in\omega L/c}|0_{\mathrm{Q}}\rangle$ and $|1_{\mathrm{Q}}\rangle \to e^{i(n\omega L/c+\phi)}|1_{\mathrm{Q}}\rangle$. This correspond, up to a global phase of $e^{in\omega L/c}$, to the gate matrix

$$R(\phi) = \begin{pmatrix} 1 & 0 \\ 0 & e^{i\phi} \end{pmatrix}, \tag{2.22}$$

which is referred to as the phase shifter gate.

Another important component in photonic quantum computing is the beam splitter, which reflects a fraction of $R = \cos^2\theta$ from incident photons and transmits a fraction of $T = 1 - R$. Here, the angle θ is the mixing angle, which can be tuned by changing the reflectivity of the reflecting surface. Beam splitter operates on two spatially separated input modes $\hat{a}^\dagger_{0,\mathrm{in}}$ and $\hat{a}^\dagger_{1,\mathrm{in}}$. The corresponding quantum gate for the beam splitter operator $\hat{B}$ in the dual-rail basis is given by [13]

$$B(\theta) = \begin{pmatrix} \cos\theta & -\sin\theta \\ \sin\theta & \cos\theta \end{pmatrix}. \tag{2.23}$$

Beam splitters with constant angle $\theta = \pi/4$ are referred to as 50:50 beam splitters since the reflected and transmitted fractions are the same, $R = T = 0.5$. With phase shifters and a beam splitter, one can construct the general 2×2 unitary matrix up to a global phase, corresponding to arbitrary single-qubit operations, by

$$U = R(\varphi_3 + \pi)B(\theta)R(\varphi_2 - \pi) = \begin{pmatrix} \cos\theta & \sin\theta e^{i\varphi_2} \\ -\sin\theta e^{i\varphi_3} & \cos\theta e^{i(\varphi_2+\varphi_3)} \end{pmatrix}. \tag{2.24}$$

In a programmable quantum computer the angle θ should be tunable. However, it may not be convenient to change the reflectivity in the beam splitter in practice. Due to this, we show how to construct the general 2×2 unitary matrix with only tunable phase shifters and constant 50:50 beam splitters. The unitary matrix U is constructed, up to a global phase, with

$$\begin{aligned} U &= R(\varphi_3 - \frac{\pi}{2})B(\pi/4)R(2\theta + \pi)B(\pi/4)R(\varphi_2 + \frac{3\pi}{2}) \\ &= e^{-i\theta}\begin{pmatrix} \cos\theta & \sin\theta e^{i\varphi_2} \\ -\sin\theta e^{i\varphi_3} & \cos\theta e^{i(\varphi_2+\varphi_3)} \end{pmatrix}. \end{aligned} \tag{2.25}$$

For a universal set of quantum gates, an entangling two-qubit gate is also required. One way to realize an entangling two-qubit gate is to utilize the nonlinearity generated by the so-called Kerr medium. In Kerr medium, the refractive index of the material is dependent on the intensity of the electromagnetic field propagating through it. Thus, two electromagnetic pulses with equal intensity propagating through the Kerr medium simultaneously will acquire an additional phase shift compared with the case in which they propagate independently. This nonlinear phase shift can be used in the implementation of two-qubit gates. However, these materials are also highly absorptive and the nonlinear effect provided by them is not strong enough for their practical use in quantum computation [13].

2.2.3 Hong–Ou–Mandel effect

The Hong–Ou–Mandel effect is a quantum-mechanical phenomenon which states that two photons entering a 50:50 beam splitter in different modes will exit the beam splitter in the same mode [15]. In order to demonstrate this effect, let us consider two physically separated waveguides connected to a 50:50 beam splitter. Furthermore, we consider a state with two photons propagating in both of the waveguides separately. Thus, the quantum state in the input mode is given by $\hat{a}^\dagger_{0,\mathrm{in}}\hat{a}^\dagger_{1,\mathrm{in}}\left|00\right\rangle = \left|11\right\rangle_{\mathrm{in}}$, where $\left|00\right\rangle$ is the vacuum state with zero photons in both modes. Interaction with the beam splitter corresponds to the gate matrix $B(\pi/4)$ defined by Eq. (2.23), yielding the mapping

$$\hat{a}^\dagger_{0,\mathrm{in}} \to \frac{1}{\sqrt{2}}\left(\hat{a}^\dagger_{0,\mathrm{out}} - \hat{a}^\dagger_{1,\mathrm{out}}\right), \tag{2.26}$$

$$\hat{a}^\dagger_{1,\mathrm{in}} \to \frac{1}{\sqrt{2}}\left(\hat{a}^\dagger_{0,\mathrm{out}} + \hat{a}^\dagger_{1,\mathrm{out}}\right), \tag{2.27}$$

where $\hat{a}^\dagger_{0,\mathrm{out}}$ and $\hat{a}^\dagger_{1,\mathrm{out}}$ are the creation operators for the output modes. The initial quantum state transforms as

$$\begin{aligned}\left|11\right\rangle_{\mathrm{in}} = \hat{a}^\dagger_{0,\mathrm{in}}\hat{a}^\dagger_{1,\mathrm{in}}\left|00\right\rangle &\to \frac{1}{2}\left(\hat{a}^\dagger_{0,\mathrm{out}} - \hat{a}^\dagger_{1,\mathrm{out}}\right)\left(\hat{a}^\dagger_{0,\mathrm{out}} + \hat{a}^\dagger_{1,\mathrm{out}}\right)\left|00\right\rangle \\ &= \frac{1}{2}\left[\left(\hat{a}^\dagger_{0,\mathrm{out}}\right)^2 - \left(\hat{a}^\dagger_{1,\mathrm{out}}\right)^2 + \hat{a}_{0,\mathrm{out}}\hat{a}_{1,\mathrm{out}} - \hat{a}_{1,\mathrm{out}}\hat{a}_{0,\mathrm{out}}\right]\left|00\right\rangle \\ &= \frac{1}{2}\left[\left(\hat{a}^\dagger_{0,\mathrm{out}}\right)^2 - \left(\hat{a}^\dagger_{1,\mathrm{out}}\right)^2\right]\left|00\right\rangle = \frac{1}{\sqrt{2}}\left(\left|20\right\rangle_{\mathrm{out}} - \left|02\right\rangle_{\mathrm{out}}\right).\end{aligned} \tag{2.28}$$

Here, we have used the fact that $\hat{a}^\dagger_{0,\mathrm{out}}$ and $\hat{a}^\dagger_{1,\mathrm{out}}$ commute since they correspond to physically separated modes. It is evident from Eq. (2.28) that for

two photons entering a 50:50 beam splitter in different modes, the output state is a superposition state in which two photons propagate in the same mode.

2.3 Superconducting qubits

Superconducting qubits are mesoscopic superconducting circuits, in which the quantum degrees of freedom appear in electric quantities, such as in charge or phase. In practice, superconducting qubits involve multiple energy levels due to their macroscopic nature. However, they can be implemented with such parameters that only two of these energy levels are relevant, hence validating their use as qubits.

2.3.1 Superconductivity

A superconducting phase, where the material exhibits exactly zero resistance, appears in some materials if the temperature is lowered below the material-dependent critical temperature. In the superconducting phase, there is an effective attractive force between the conduction electrons, and hence they tend to form pairs. These pairs are commonly referred to as Cooper pairs. The origin of the attractive force is typically due to electron–phonon interactions in the superconducting materials. [16]

In conventional superconductors, the total spin of a single Cooper pair is zero and multiple Cooper pairs condense into the same quantum state with properties similar to those of Bose-Einstein condensates. In the mean-field approximation, the superfluid is described by an order parameter

$$\Psi(\mathbf{r}) = |\Psi(\mathbf{r})|\, e^{i\phi(\mathbf{r})}, \tag{2.29}$$

where $\phi(\mathbf{r})$ is the complex phase factor. [17]

2.3.2 Josephson junction

Cooper pairs may tunnel from one superconductor to another through a weak link between them. The weak link could be, for example, normal metal or an insulator. This device is called a Josephson junction and it is the source of anharmonicity in the energy levels of superconducting qubits, rendering it an essential component in the field of circuit quantum electrodynamics.

The time evolutions of voltage and current through the Josephson junction are governed by the Josephson relations

$$V(t) = \frac{\Phi_0}{2\pi}\frac{\partial\varphi(t)}{\partial t}, \tag{2.30}$$

$$I(t) = I_\mathrm{c}\sin\varphi(t), \tag{2.31}$$

where $\Phi_0 = h/(2e)$ is the magnetic flux quantum, $\varphi = \phi_2 - \phi_1$ is the phase difference between the two superconductors, and I_c is the critical current. The energy of the system is calculated by integrating the power $I(t)V(t)$ over time, yielding

$$U_\mathrm{J}(\varphi) = -E_\mathrm{J}\cos\varphi, \tag{2.32}$$

where the Josephson energy is defined as $E_\mathrm{J} = \Phi_0 I_\mathrm{c}/(2\pi)$.

2.3.3 Cooper pair box

The circuit diagram of the Cooper pair box (CPB) design of the superconducting qubit is presented in Fig. 2.1. In this design, a gate capacitor with capacitance C_g and a Josephson junction with capacitance C_J form a superconducting island between them. The Cooper pairs may tunnel through the junction to the island, and in the CPB design, the number of excess Cooper pairs on the island, N, is used to form the basis $\{|N\rangle\}$ with $|N\rangle$ being a state with N excess pairs on the island. This basis is referred to as the charge basis, since N is proportional to the total charge on the island. In this basis, the CPB Hamiltonian is given by [18]

$$\begin{aligned}\hat{\mathcal{H}}_\mathrm{CPB} = \sum_N \Big[& 4E_\mathrm{C}(N-n_\mathrm{g})^2 |N\rangle\langle N| \\ & -\frac{E_\mathrm{J}}{2}(|N\rangle\langle N+1| + |N+1\rangle\langle N|)\Big],\end{aligned} \tag{2.33}$$

where $E_\mathrm{C} = e^2/[2(C_\mathrm{g}+C_\mathrm{J})]$ is the charging energy of the island and $n_\mathrm{g} = C_\mathrm{g}V_\mathrm{g}/(2e)$ is the normalized gate charge. In order to justify the two-level approximation, the number of Cooper pairs N need to be restricted to two values, i.e., we must have $E_\mathrm{C} \gg E_\mathrm{J}$ as well as $|n_\mathrm{g} - 1/2 + k| < 1/2$, where $k \in \mathbb{Z}$ [18].

2.3.4 Transmon

The charge basis for the CPB design is well-defined in the regime where $E_\mathrm{C} \gg E_\mathrm{J}$. In contrast to the CPB, in the regime where $E_\mathrm{C} \ll E_\mathrm{J}$, the

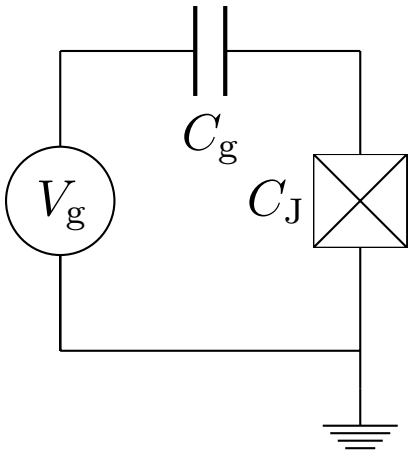

Figure 2.1: Circuit diagram of the Cooper pair box. The capacitances for the gate capacitor and the Josephson junction are given by C_g and C_J, respectively. The circuit contains an external voltage source of voltage V_g.

charge states cannot be used as a basis for qubit. For the similar design as is used in the CPB, this limit corresponds to the so-called transmon qubit. The benefits of this design are the reduced sensitivity to the external charge noise as well as the increased coupling strength between the qubits and the microwave photons in the transmission line. [19]

In the limit where $E_\mathrm{J}/E_\mathrm{C}$ is large, the transmon can be approximated as a harmonic oscillator with a small perturbation. By increasing the ratio $E_\mathrm{J}/E_\mathrm{C}$, the sensitivity to the charge noise decreases exponentially and the anharmonicity in the energy levels decreases with a power law as $(E_\mathrm{J}/E_\mathrm{C})^{1/2}$. Remarkably, the coupling strength between the transmon and the microwave field in the transmission line is increased with increasing ratio $E_\mathrm{J}/E_\mathrm{C}$. [19]

2.4 Quantum optics

2.4.1 Jaynes–Cummings model

Quantum optics provides tools that can be directly applied in circuit quantum electrodynamics, where the interest lies in the interactions between the electromagnetic field (microwave photons) and matter (superconducting qubits). Introducing the creation and annihilation operators, $\hat{a}_k^\dagger$ and $\hat{a}_k$, for a photon with wavenumber k in one-dimensional space, the electromagnetic field is

written as a sum of infinitely many harmonic oscillators [20]

$$\hat{\mathcal{H}}_{\mathrm{em}} = \sum_k \hbar\omega_k \left(\hat{a}_k^\dagger \hat{a}_k + \frac{1}{2}\right). \tag{2.34}$$

Let us assume that the photons reside in a resonator cavity with a high quality factor. This system is effectively described as an electromagnetic field with a single mode of frequency ω. Furthermore, we assume that a superconducting qubit with transition frequency Ω is coupled to the system, interacting with the cavity field. The energy eigenstates of the qubit are $|\mathrm{g}\rangle$ and $|\mathrm{e}\rangle$, corresponding to the ground and excited states, respectively. The system is described in the Schrödinger picture by the Hamiltonian [21]

$$\hat{\mathcal{H}}^{\mathrm{S}} = \hbar\omega\hat{a}^\dagger\hat{a} + \frac{1}{2}\hbar\Omega\hat{\sigma}_z + \hbar g\left(\hat{a} + \hat{a}^\dagger\right)\left(\hat{\sigma}_+ + \hat{\sigma}_-\right), \tag{2.35}$$

where $\hat{\sigma}_z = |\mathrm{e}\rangle\langle\mathrm{e}| - |\mathrm{g}\rangle\langle\mathrm{g}|$, $\hat{\sigma}_+ = |\mathrm{e}\rangle\langle\mathrm{g}|$, $\hat{\sigma}_- = (\hat{\sigma}_+)^\dagger$, and g is the coupling strength. Separating the noninteracting and interacting parts of the Hamiltonian as $\hat{\mathcal{H}}_0^{\mathrm{S}} = \hbar\omega\hat{a}^\dagger\hat{a} + \frac{1}{2}\hbar\Omega\hat{\sigma}_z$ and $\hat{\mathcal{H}}_{\mathrm{int}}^{\mathrm{S}} = \hbar g\left(\hat{a} + \hat{a}^\dagger\right)(\hat{\sigma}_+ + \hat{\sigma}_-)$, we obtain the Hamiltonian in the interaction picture

$$\begin{aligned}\hat{\mathcal{H}}^{\mathrm{I}}(t) =& \hbar g\left[\hat{a}\hat{\sigma}_- e^{-i(\omega+\Omega)t} + \hat{a}^\dagger\hat{\sigma}_+ e^{i(\omega+\Omega)t}\right.\\ &\left.+\hat{a}\hat{\sigma}_+ e^{-i(\omega-\Omega)t} + \hat{a}^\dagger\hat{\sigma}_- e^{i(\omega-\Omega)t}\right].\end{aligned} \tag{2.36}$$

The Jaynes–Cummings (JC) model is obtained in the limit where the rotating-wave approximation (RWA) is valid, i.e., $|\omega - \Omega| \ll \omega + \Omega$. In this limit, we may neglect the first two terms in Hamiltonian (2.36) since they are quickly oscillating and hence average out. Transforming back to the Schrödinger picture, we write the JC Hamiltonian as

$$\hat{\mathcal{H}}_{\mathrm{JC}}^{\mathrm{S}} = \hbar\omega\hat{a}^\dagger\hat{a} + \frac{1}{2}\hbar\Omega\hat{\sigma}_z + \hbar g\left(\hat{a}\hat{\sigma}_+ + \hat{a}^\dagger\hat{\sigma}_-\right). \tag{2.37}$$

2.4.2 Dispersive limit

In case the detuning between the atom and the electromagnetic field frequencies is large, the system is referred to as being in the dispersive limit. In this limit, the coupling strength g satisfies $g \ll |\omega - \Omega| \equiv \Delta$. Within the RWA, performing the unitary transformation $\hat{U} = \exp\left[g/\Delta\left(\hat{a}\hat{\sigma}_+ - \hat{a}^\dagger\hat{\sigma}_-\right)\right]$ to the JC Hamiltonian of Eq. (2.37) provides us with [10]

$$\mathcal{H}_{\mathrm{JC,disp}}^{\mathrm{S}} \equiv \hat{U}\mathcal{H}_{\mathrm{JC}}^{\mathrm{S}}\hat{U}^\dagger = \hbar\omega\hat{a}^\dagger\hat{a} + \frac{\hbar}{2}\left[\Omega + \frac{g^2}{\Delta}\left(2\hat{a}^\dagger\hat{a} + 1\right)\right]\hat{\sigma}_z + \mathcal{O}(g^4). \tag{2.38}$$

We note that the effective transition frequency of the qubit depends on the number of photons as

$$\Omega_{\text{eff}} = \Omega + \frac{g^2}{\Delta}\left(2n+1\right), \tag{2.39}$$

where n is the number of photons. The creation of entangling multi-qubit gates based on this type of nonlinearity has been considered [12].

2.4.3 Input-output theory

The theory relating the incoming and outgoing fields radiated by the cavity is known as the quantum input-output theory. As an example of the theory, let us study the case where a cavity is placed between two one-dimensional semi-infinite waveguides. The input-output relations for such a system are given by [20]

$$\hat{b}_{\text{out}}(t) = \sqrt{\kappa_1}\hat{a}(t) - \hat{b}_{\text{in}}(t), \tag{2.40}$$

$$\hat{c}_{\text{out}}(t) = \sqrt{\kappa_2}\hat{a}(t) - \hat{c}_{\text{in}}(t), \tag{2.41}$$

where the annihilation operators are given by $\hat{b}_{\text{out}}(t)$, $\hat{b}_{\text{in}}(t)$ for the outgoing and incoming waves in the left waveguide, $\hat{c}_{\text{out}}(t)$, $\hat{c}_{\text{in}}(t)$ for the outgoing and incoming waves in the right waveguide, and $\hat{a}(t)$ for the cavity field. The constants κ_1 and κ_2 are the decay rates to the left and right waveguides, respectively. If a qubit is coupled to the cavity, the cavity mode evolves according to the quantum Langevin equation, given by [22]

$$\frac{d\hat{a}(t)}{dt} = -\frac{i}{\hbar}\left[\hat{a}(t), \hat{\mathcal{H}}\right] - \left(\frac{\kappa_1}{2} + \frac{\kappa_2}{2}\right)\hat{a}(t) + \sqrt{\kappa_1}\hat{b}_{\text{in}}(t) + \sqrt{\kappa_2}\hat{c}_{\text{in}}(t), \tag{2.42}$$

where $\hat{\mathcal{H}}$ is the Hamiltonian for the cavity–qubit system. As an example, in the dispersive limit the Hamiltonian is given by Eq. (2.38). Within this limit, neglecting the quartic and higher order terms, the evolution given by Eq. (2.42) can be solved in frequency space by taking Fourier transformations of Eqs. (2.40)–(2.42) [22]. Furthermore, it can be shown that the phase shift between the output field $\hat{c}_{\text{out}}(\omega)$ and the input field $\hat{b}_{\text{in}}(\omega)$ in the dispersive limit with a single qubit coupled to the cavity is expressed as

$$\phi = \arctan\left[\frac{2\left(\omega_{\text{r}} - \omega + g^2/\Delta\,\langle\hat{\sigma}_z\rangle\right)}{\kappa_1 + \kappa_2}\right], \tag{2.43}$$

where ω_{r} is the resonance frequency of the cavity and ω is the frequency of the photons. Depending on whether the qubit coupled to the cavity is excited ($\langle\hat{\sigma}_z\rangle = 1$) or in the ground state ($\langle\hat{\sigma}_z\rangle = -1$), there appears a qubit state-dependent shift in the phase of the transmitted photons.

Chapter 3

Methods: waveguide quantum electrodynamics

In this chapter, we derive the quantum-electrodynamical Hamiltonian for an infinite superconducting transmission line, to which an arbitrary number of superconducting qubits are capacitively coupled. The derivation follows Ref. [23], but with intermediate results as well as the quantization procedure explicitly written down. Finally, we represent the Hamiltonian of the system in terms of the field operators of the photons and briefly discuss how dissipation could be included in the model.

3.1 Distributed-element model

We consider an infinite transmission line, to which N superconducting islands are capacitively coupled at locations x_j, where j indexes the islands. We assume that the islands do not overlap, i.e., $x_j \neq x_{j'}$, for $j \neq j'$. Physically, a typical transmission line consists of a centre conductor capacitively coupled to an outer conductor that is connected to the ground. Here, we model the transmission line as an infinite series of LC units of length Δx consisting of capacitors with capacitances $C = c\Delta x$ and inductors with inductances $L = l\Delta x$, where l and c are inductance and capacitance per unit length of the transmission line, respectively. The inductors are connected in series and the capacitors are connected to the ground from the nodes in which two adjacent inductors connect. Our model does not include any dissipative elements in the transmission line, since we assume that the transmission line is lossless.

The jth superconducting island is modeled with a gate capacitor with capacitance $C_{\mathrm{G},j}$ and a Josephson junction with capacitance $C_{\mathrm{J},j}$. The Joseph-

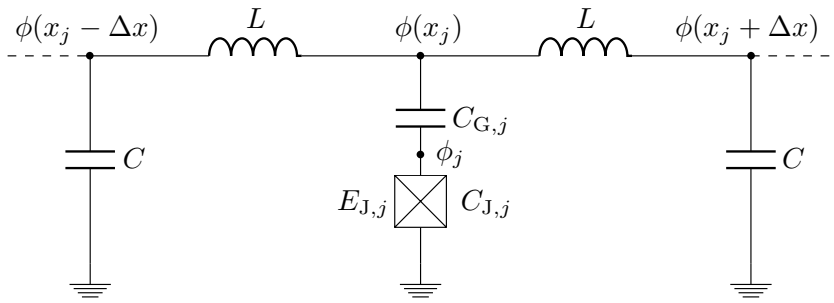

Figure 3.1: Distributed-element representation of a circuit where a superconducting qubit is coupled to an infinite transmission line at location x_j.

son junction acts as a nonlinear element with the Josephson energy $E_{\mathrm{J},j}$. In the quantization procedure (presented in Sec. 3.3.2), we observe that the degrees of freedom related to such a superconducting island can be approximated by those of a two-level quantum system. Hence, the islands are hereby referred to as superconducting qubits, or simply qubits.

The equivalent circuit diagram for the transmission line in the neighborhood of the node where the jth qubit is coupled is presented in Fig. 3.1. Since the circuit includes a Josephson junction, we take the generalized fluxes at the superconducting islands, ϕ_j, and in the transmission line, $\phi(n\Delta x)$, as the coordinates for our system. The generalized flux is defined as the time integral of the voltage across the corresponding element from the distant past, when all electromagnetic fields in the circuit were zero, to the current time [24]. The Lagrangian for the complete system is constructed as [23]

$$\begin{aligned}\mathcal{L} = &\sum_{n=-\infty}^{\infty} \left\{ \frac{C}{2}\dot{\phi}(n\Delta x)^2 - \frac{\{\phi\left[(n+1)\Delta x\right] - \phi(n\Delta x)\}^2}{2L} \right\} \\ &+ \sum_{j=0}^{N-1} \left\{ \frac{C_{\mathrm{G},j}}{2}\left[\dot{\phi}(x_j) - \dot{\phi}_j\right]^2 + \left[\frac{C_{\mathrm{J},j}}{2}\dot{\phi}_j^2 + E_{\mathrm{J},j}\cos\left(\frac{2\pi}{\Phi_0}\phi_j\right)\right] \right\}, \end{aligned} \tag{3.1}$$

where the magnetic flux quantum is given by $\Phi_0 = h/(2e)$, h is the Planck's constant, and e is the elementary charge. We include the transmission line capacitors with capacitances C in the description even for the indices corresponding to qubits. By doing this, we can, when approximating different effective capacitances, take into account the finite length of the superconducting qubits [23].

The charges $Q(n\Delta x)$ and Q_j are the canonical conjugate variables of fluxes $\phi(n\Delta x)$ and ϕ_j, respectively, and they can be calculated by taking the

following variations of the Lagrangian [24]:

$$Q_j = \frac{\delta \mathcal{L}}{\delta \dot{\phi}_j} = -C_{\mathrm{G},j}\left[\dot{\phi}(x_j) - \dot{\phi}_j\right] + C_{\mathrm{J},j}\dot{\phi}_j, \tag{3.2}$$

$$Q(x_j) = \frac{\delta \mathcal{L}}{\delta \dot{\phi}(x_j)} = C\dot{\phi}(x_j) + C_{\mathrm{G},j}\left[\dot{\phi}(x_j) - \dot{\phi}_j\right], \tag{3.3}$$

$$Q(n\Delta x) = \frac{\delta \mathcal{L}}{\delta \dot{\phi}(n\Delta x)} = C\dot{\phi}(n\Delta x), n \neq \frac{x_j}{\Delta x}. \tag{3.4}$$

Rewriting the above equations for the derivatives of the fluxes, we obtain

$$\dot{\phi}_j = \frac{CQ_j + C_{\mathrm{G},j}\left[Q_j + Q(x_j)\right]}{C_{\mathrm{G},j}C_{\mathrm{J},j} + C\left(C_{\mathrm{G},j} + C_{\mathrm{J},j}\right)}, \tag{3.5}$$

$$\dot{\phi}(x_j) = \frac{C_{\mathrm{J},j}Q(x_j) + C_{\mathrm{G},j}\left[Q_j + Q(x_j)\right]}{C_{\mathrm{G},j}C_{\mathrm{J},j} + C\left(C_{\mathrm{G},j} + C_{\mathrm{J},j}\right)}, \tag{3.6}$$

$$\dot{\phi}(n\Delta x) = \frac{Q(n\Delta x)}{C}, n \neq \frac{x_j}{\Delta x}. \tag{3.7}$$

The Hamiltonian is defined as the Legendre transformation of the Lagrangian, and using Eqs. (3.5)–(3.7), the Hamiltonian becomes

$$\begin{aligned}
\mathcal{H} =& \sum_n \dot{\phi}(n\Delta x)Q(n\Delta x) + \sum_{j=0}^{N-1}\dot{\phi}_j Q_j - \mathcal{L} \\
=& \sum_{n\neq j}\frac{Q(n\Delta x)^2}{2C} + \sum_n\left\{\frac{\left\{\phi\left[(n+1)\Delta x\right] - \phi(n\Delta x)\right\}^2}{2L}\right\} \\
&+ \sum_{j=0}^{N-1}\left[Q(x_j)^2\frac{C_{\mathrm{G},j} + C_{\mathrm{J},j}}{2C_{\mathrm{G},j}C_{\mathrm{J},j} + 2C(C_{\mathrm{G},j} + C_{\mathrm{J},j})}\right. \\
&+ Q(x_j)Q_j\frac{C_{\mathrm{G},j}}{C_{\mathrm{G},j}C_{\mathrm{J},j} + C(C_{\mathrm{G},j} + C_{\mathrm{J},j})} \\
&+ Q_j^2\frac{C + C_{\mathrm{G},j}}{2C_{\mathrm{G},j}C_{\mathrm{J},j} + 2C(C_{\mathrm{G},j} + C_{\mathrm{J},j})} \\
&\left.- E_{\mathrm{J},j}\cos\left(\frac{2\pi}{\Phi_0}\phi_j\right)\right] \\
=& \sum_n\left\{\frac{Q(n\Delta x)^2}{2C_{\Sigma,\mathrm{TL}}(n\Delta x)} + \frac{\left\{\phi\left[(n+1)\Delta x\right] - \phi(n\Delta x)\right\}^2}{2L}\right\} \\
&+ \sum_{j=0}^{N-1}\left[\frac{Q_j^2}{2C_{\Sigma,j}} + \frac{Q(x_j)Q_j}{2C_{\mathrm{c},j}} - E_{\mathrm{J},j}\cos\left(\frac{2\pi}{\Phi_0}\phi_j\right)\right].
\end{aligned} \tag{3.8}$$

Here, the effective capacitance on the transmission line is defined as

$$C_{\Sigma,\mathrm{TL}}(n\Delta x) = C + \sum_{j=0}^{N-1} \frac{C_{\mathrm{G},j}C_{\mathrm{J},j}}{C_{\mathrm{G},j}+C_{\mathrm{J},j}}\delta_{n\Delta x,x_j}, \tag{3.9}$$

where δ_{ij} is the Kronecker delta. In this formulation of the Hamiltonian, we have also defined the effective total and the coupling capacitances of the qubits as

$$C_{\Sigma,j} = \frac{C_{\mathrm{G},j}C_{\mathrm{J},j} + C(C_{\mathrm{G},j}+C_{\mathrm{J},j})}{C+C_{\mathrm{G},j}}, \tag{3.10}$$

$$C_{\mathrm{c},j} = \frac{C_{\mathrm{G},j}C_{\mathrm{J},j} + C(C_{\mathrm{G},j}+C_{\mathrm{J},j})}{2C_{\mathrm{G},j}}. \tag{3.11}$$

3.2 Continuum limit

Transmission line capacitances and inductances are in practice expressed as $C = c\Delta x$ and $L = l\Delta x$, where c and l are the capacitance and inductance per unit length of the transmission line, respectively. In the continuum limit, we let $\Delta x \to 0$. The finite length of the superconducting islands is taken into account by making an exception at the qubit sites x_j, where we take $\Delta x \to d_{\mathrm{J}}$, where d_{J} is the length of a single island [23].

In the continuum limit, the charge density q and the flux ϕ transform to functions with a continuous position variable x as $q(n\Delta x) = Q(n\Delta x)/\Delta x \to q(x)$ and $\phi(n\Delta x) \to \phi(x)$. The average effective capacitance per unit length on the transmission line transforms as $C_{\Sigma,\mathrm{TL}}(n\Delta x)/\Delta x \to c_{\Sigma,\mathrm{TL}}(x)$. We approximate that the capacitance of the transmission line dominates the capacitances related to the qubit sites, and write the effective transmission line capacitance per unit length as $c_{\Sigma,\mathrm{TL}}(x) \approx c$ [23]. The effective total capacitance and the effective coupling capacitance per unit length transform in the continuum limit as

$$C_{\Sigma,j} \to \frac{C_{\mathrm{G},j}C_{\mathrm{J},j} + cd_{\mathrm{J}}(C_{\mathrm{G},j}+C_{\mathrm{J},j})}{cd_{\mathrm{J}}+C_{\mathrm{G},j}}, \tag{3.12}$$

$$C_{\mathrm{c},j}/\Delta x \to c_{\mathrm{c},j} = \frac{C_{\mathrm{G},j}C_{\mathrm{J},j}/d_{\mathrm{J}} + c(C_{\mathrm{G},j}+C_{\mathrm{J},j})}{2C_{\mathrm{G},j}}. \tag{3.13}$$

Finally, the Hamiltonian describing N qubits capacitively coupled to the

transmission line can be approximated in the continuum limit as

$$\mathcal{H} \approx \int_{-\infty}^{\infty} dx \Bigg\{ \frac{q(x)^2}{2c} + \frac{1}{2l}\left[\frac{\partial\phi(x)}{\partial x}\right]^2 + \sum_{j=0}^{N-1} \delta(x-x_j)\left[\frac{Q_j^2}{2C_{\Sigma,j}} + \frac{Q_j q(x)}{c_{\mathrm{c},j}} - E_{\mathrm{J},j}\cos\left(\frac{2\pi}{\Phi_0}\phi_j\right)\right]\Bigg\}. \tag{3.14}$$

3.3 Quantization

We quantize the system by promoting the transmission line charge density q and the flux ϕ into operators $\hat{q}$ and $\hat{\phi}$, respectively. We also promote the charges Q_j and fluxes ϕ_j at the superconducting islands into operators $\hat{Q}_j$ and $\hat{\phi}_j$, respectively. The Hamiltonian (3.14) becomes an operator $\hat{\mathcal{H}}$ in the quantization procedure

$$\hat{\mathcal{H}} = \hat{\mathcal{H}}_{\mathrm{TL}} + \sum_{j=0}^{N-1}\left(\hat{\mathcal{H}}_{\mathrm{q},j} + \hat{\mathcal{H}}_{\mathrm{c},j}\right), \tag{3.15}$$

$$\hat{\mathcal{H}}_{\mathrm{TL}} = \int_{-\infty}^{\infty} dx \left\{ \frac{\hat{q}(x)^2}{2c} + \frac{1}{2l}\left[\frac{\partial\hat{\phi}(x)}{\partial x}\right]^2 \right\}, \tag{3.16}$$

$$\hat{\mathcal{H}}_{\mathrm{q},j} = \frac{\hat{Q}_j^2}{2C_{\Sigma,j}} - E_{\mathrm{J},j}\cos\left(\frac{2\pi}{\Phi_0}\hat{\phi}_j\right), \tag{3.17}$$

$$\hat{\mathcal{H}}_{\mathrm{c},j} = \frac{\hat{Q}_j\hat{q}(x_j)}{c_{\mathrm{c},j}}, \tag{3.18}$$

where the Hamiltonian operators $\hat{\mathcal{H}}_{\mathrm{TL}}$, $\hat{\mathcal{H}}_{\mathrm{q},j}$, and $\hat{\mathcal{H}}_{\mathrm{c},j}$ are associated with the transmission line, jth qubit, and their coupling, respectively.

3.3.1 Transmission line

We employ the Heisenberg picture for the charge density operator $\hat{q}$ and the flux operator $\hat{\phi}$ of a bare transmission line, and hence they become time-dependent. The operators in the Heisenberg picture are labeled with the superscript H and the operators in the Schrödinger picture are left unlabeled. These operators are also canonical conjugate variables to each other, and

hence satisfy the following equal-time commutation relations

$$\left[\hat{\phi}^{\mathrm{H}}(x,t),\hat{\phi}^{\mathrm{H}}(x',t)\right]=0, \tag{3.19}$$

$$\left[\hat{q}^{\mathrm{H}}(x,t),\hat{q}^{\mathrm{H}}(x',t)\right]=0, \tag{3.20}$$

$$\left[\hat{\phi}^{\mathrm{H}}(x,t),\hat{q}^{\mathrm{H}}(x',t)\right]=i\hbar\delta(x-x'). \tag{3.21}$$

Using Eqs. (3.19)–(3.21), the Heisenberg equations of motion for the charge density operator in the bare transmission line at $x \neq x_j$ becomes

$$\begin{aligned}
\frac{\partial}{\partial t}\hat{q}^{\mathrm{H}}(x,t) &= -\frac{i}{\hbar}\left[\hat{q}^{\mathrm{H}}(x,t),\hat{\mathcal{H}}_{\mathrm{TL}}\right] \\
&= -\frac{i}{\hbar}\int_{-\infty}^{\infty}dx'\Bigg\{\frac{1}{2c}\left[\hat{q}^{\mathrm{H}}(x,t),\hat{q}^{\mathrm{H}}(x',t)^2\right] \\
&\quad + \frac{1}{2l}\left[\hat{q}^{\mathrm{H}}(x,t),\left(\frac{\partial}{\partial x'}\hat{\phi}^{\mathrm{H}}(x',t)\right)^2\right]\Bigg\} \\
&= -\frac{i}{2l\hbar}\int_{-\infty}^{\infty}dx'\left[\hat{q}^{\mathrm{H}}(x,t),\left(\frac{\partial}{\partial x'}\hat{\phi}^{\mathrm{H}}(x',t)\right)^2\right] \\
&= -\frac{i}{2l\hbar}\int_{-\infty}^{\infty}dx'\left[\left[\hat{q}^{\mathrm{H}}(x,t),\frac{\partial}{\partial x'}\hat{\phi}^{\mathrm{H}}(x',t)\right],\frac{\partial}{\partial x'}\hat{\phi}^{\mathrm{H}}(x',t)\right]_+ \\
&= \frac{i}{2l\hbar}\int_{-\infty}^{\infty}dx'\left[\left[\hat{q}^{\mathrm{H}}(x,t),\hat{\phi}^{\mathrm{H}}(x',t)\right],\frac{\partial^2}{\partial x'^2}\hat{\phi}^{\mathrm{H}}(x',t)\right]_+ \\
&= -\frac{i}{2l\hbar}\int_{-\infty}^{\infty}dx'\,2i\hbar\delta(x-x')\frac{\partial^2}{\partial x'^2}\hat{\phi}^{\mathrm{H}}(x',t) \\
&= \frac{1}{l}\frac{\partial^2}{\partial x^2}\hat{\phi}^{\mathrm{H}}(x,t),
\end{aligned} \tag{3.22}$$

where $[A,B]_+ = AB + BA$ is the anticommutator. On the rows five and six we have integrated by parts, used $\partial_{x'}\hat{q}^{\mathrm{H}}(x,t)=0$, and made the assumption $\lim_{x\to\pm\infty}\hat{\phi}^{\mathrm{H}}(x,t)=0$. The equation of motion for the flux operator is

calculated similarly:

$$\begin{aligned}
\frac{\partial}{\partial t}\hat{\phi}^{\mathrm{H}}(x,t) &= -\frac{i}{\hbar}\left[\hat{\phi}^{\mathrm{H}}(x,t), \hat{\mathcal{H}}_{\mathrm{TL}}\right] \\
&= -\frac{i}{\hbar}\int_{-\infty}^{\infty} dx' \Bigg\{ \frac{1}{2c}\left[\hat{\phi}^{\mathrm{H}}(x,t), \hat{q}^{\mathrm{H}}(x',t)^2\right] \\
&\quad + \frac{1}{2l}\left[\hat{\phi}^{\mathrm{H}}(x,t), \left[\frac{\partial}{\partial x'}\hat{\phi}^{\mathrm{H}}(x',t)\right]^2\right]\Bigg\} \\
&= -\frac{i}{2c\hbar}\int_{-\infty}^{\infty} dx' \left[\hat{\phi}^{\mathrm{H}}(x,t), \hat{q}^{\mathrm{H}}(x',t)^2\right] \\
&= -\frac{i}{2c\hbar}\int_{-\infty}^{\infty} dx' \left[\left[\hat{\phi}^{\mathrm{H}}(x,t), \hat{q}^{\mathrm{H}}(x',t)\right], \hat{q}^{\mathrm{H}}(x',t)\right]_+ \\
&= -\frac{i}{2c\hbar}\int_{-\infty}^{\infty} dx' \, 2i\hbar\delta(x-x')\hat{q}^{\mathrm{H}}(x',t) \\
&= \frac{1}{c}\hat{q}^{\mathrm{H}}(x,t). \qquad (3.23)
\end{aligned}$$

We take the time derivative on both sides of Eq. (3.22) and the spatial derivative twice on both sides of Eq. (3.23). Equating the obtained derivatives for the flux operator leads to the wave equation

$$l\frac{\partial^2}{\partial t^2}\hat{q}^{\mathrm{H}}(x,t) = \frac{1}{c}\frac{\partial^2}{\partial x^2}\hat{q}^{\mathrm{H}}(x,t). \qquad (3.24)$$

We assume that the photonic dispersion can be linearized, such that $\omega = v\,|k|$, where v is the group velocity and k is the wavenumber of the photons. Thus, the general solution for the charge density and the flux operators in the Heisenberg picture can be expressed as [25]

$$\hat{q}^{\mathrm{H}}(x,t) = c\sqrt{\frac{\hbar Z_0}{4\pi}}\int_0^{\infty} d\omega\sqrt{\omega}\left[\hat{a}_{\mathrm{L}}(\omega)e^{-i\omega(t+x/v)} + \hat{a}_{\mathrm{R}}(\omega)e^{-i\omega(t-x/v)} + \mathrm{h.c.}\right], \qquad (3.25)$$

$$\hat{\phi}^{\mathrm{H}}(x,t) = -i\sqrt{\frac{\hbar Z_0}{4\pi}}\int_0^{\infty} d\omega\frac{1}{\sqrt{\omega}}\left[\hat{a}_{\mathrm{L}}(\omega)e^{-i\omega(t+x/v)} + \hat{a}_{\mathrm{R}}(\omega)e^{-i\omega(t-x/v)} - \mathrm{h.c.}\right], \qquad (3.26)$$

where h.c. denotes the Hermitian conjugate, $Z_0 = \sqrt{l/c}$ is the characteristic impedance of the transmission line, and $v = 1/\sqrt{lc}$ is the photonic group velocity in the transmission line. The time-independent creation and annihilation operators for left and right propagating photons with angular

frequency ω are given by $\hat{a}^\dagger_{\mathrm{L/R}}(\omega)$ and $\hat{a}_{\mathrm{L/R}}(\omega)$, respectively, and they satisfy the bosonic commutation relations

$$\left[\hat{a}_\alpha(\omega), \hat{a}_{\alpha'}(\omega')\right] = 0, \tag{3.27}$$

$$\left[\hat{a}^\dagger_\alpha(\omega), \hat{a}^\dagger_{\alpha'}(\omega')\right] = 0, \tag{3.28}$$

$$\left[\hat{a}_\alpha(\omega), \hat{a}^\dagger_{\alpha'}(\omega')\right] = \delta_{\alpha,\alpha'}\delta(\omega - \omega'), \tag{3.29}$$

where $\alpha, \alpha' \in \{\mathrm{L}, \mathrm{R}\}$. We may insert Eqs. (3.25) and (3.26) into the transmission line Hamiltonian (3.16), and by using the bosonic commutation relations from Eqs. (3.27)–(3.29) (see Ref. [26] for explicit derivation), we arrive, up to a constant, at

$$\begin{aligned}\hat{\mathcal{H}}_{\mathrm{TL}}(t) &= \int_{-\infty}^{\infty} dx \left\{ \frac{\hat{q}^{\mathrm{H}}(x,t)^2}{2c} + \frac{1}{2l}\left[\frac{\partial \hat{\phi}^{\mathrm{H}}(x,t)}{\partial x}\right]^2 \right\} \\ &= \int_0^\infty d\omega\, \hbar\omega \left[\hat{a}^\dagger_{\mathrm{L}}(\omega)\hat{a}_{\mathrm{L}}(\omega) + \hat{a}^\dagger_{\mathrm{R}}(\omega)\hat{a}_{\mathrm{R}}(\omega)\right]. \end{aligned} \tag{3.30}$$

Assuming that the wavepackets consist of frequencies within a narrow bandwidth near ω_0, the charge density and the flux operators of Eqs. (3.25) and (3.26) become

$$\begin{aligned}\hat{q}^{\mathrm{H}}(x,t) &\approx c\sqrt{\frac{\hbar Z_0 \omega_0}{4\pi}} \int_0^\infty d\omega \left[\hat{a}_{\mathrm{L}}(\omega)e^{-i\omega(t+x/v)} + \hat{a}_{\mathrm{R}}(\omega)e^{\omega(t-x/v)} + \mathrm{h.c.}\right] \\ &= c\sqrt{\frac{\hbar Z_0 \omega_0 v}{2}} \left[\hat{a}^{\mathrm{H}}_{\mathrm{L}}(x,t) + \hat{a}^{\mathrm{H}}_{\mathrm{R}}(x,t) + \mathrm{h.c.}\right], \end{aligned} \tag{3.31}$$

$$\begin{aligned}\hat{\phi}^{\mathrm{H}}(x,t) &\approx -i\sqrt{\frac{\hbar Z_0}{4\pi\omega_0}} \int_0^\infty d\omega \left[\hat{a}_{\mathrm{L}}(\omega)e^{-i\omega(t+x/v)} + \hat{a}_{\mathrm{R}}(\omega)e^{-i\omega(t-x/v)} - \mathrm{h.c.}\right] \\ &= -i\sqrt{\frac{\hbar Z_0 v}{2\omega_0}} \left[\hat{a}^{\mathrm{H}}_{\mathrm{L}}(x,t) + \hat{a}^{\mathrm{H}}_{\mathrm{R}}(x,t) - \mathrm{h.c.}\right]. \end{aligned} \tag{3.32}$$

In this approximation, the operators are simply linear combinations of the photonic field operators, which are defined in the Heisenberg picture as [26]

$$\hat{a}^{\mathrm{H}}_{\mathrm{R/L}}(x,t) = \frac{1}{\sqrt{2\pi v}} \int_0^\infty d\omega\, \hat{a}_{\mathrm{R/L}}(\omega) e^{-i\omega(t \mp x/v)}, \tag{3.33}$$

and in the Schrödinger picture as

$$\hat{a}_{\mathrm{R/L}}(x) = \frac{1}{\sqrt{2\pi v}} \int_0^\infty d\omega\, \hat{a}_{\mathrm{R/L}}(\omega) e^{\pm i\omega x/v}. \tag{3.34}$$

Finally, we present the flux and the charge density operators within the narrow-bandwidth approximation in the Schrödinger picture as

$$\hat{q}(x) \approx c\sqrt{\frac{\hbar Z_0 \omega_0}{4\pi}} \int_0^\infty d\omega \left[\hat{a}_{\mathrm{L}}(\omega) e^{-i\omega x/v} + \hat{a}_{\mathrm{R}}(\omega) e^{i\omega x/v} + \mathrm{h.c.}\right], \tag{3.35}$$

$$\hat{\phi}(x) \approx -i\sqrt{\frac{\hbar Z_0}{4\pi\omega_0}} \int_0^\infty d\omega \left[\hat{a}_{\mathrm{L}}(\omega) e^{-i\omega x/v} + \hat{a}_{\mathrm{R}}(\omega) e^{i\omega x/v} - \mathrm{h.c.}\right]. \tag{3.36}$$

3.3.2 Superconducting qubit

In this section we first assume that the charging energy of the qubit is larger than the Josephson energy, since it is instructive to derive the two-level approximation in this limit. This parameter regime correspond to the Cooper pair box (CPB) design of the superconducting qubit, where we use the lowest two charge states on the superconducting island to define the two-level approximation. In Sec. 3.3.3, we discuss the case where the Josephson energy dominates, rendering the use of charge states as an approximation of the two-level system unjustified.

We assume that the gate capacitor of the jth superconducting island is biased by a tunable voltage $V_{\mathrm{g},j}$, which then defines the normalized gate voltage as $n_{\mathrm{g},j} = C_{\mathrm{G},j} V_{\mathrm{g},j}/(2e)$. The charge on the island of the jth qubit, Q_j, can be written in terms of the number of excess Cooper pairs on the island, n_j, and the normalized gate voltage $n_{\mathrm{g},j}$. In the quantization procedure, Q_j and n_j are promoted into operators $\hat{Q}_j$ and $\hat{n}_j$, respectively. The charge operator can be written with the number of Cooper pairs on the island and the normalized gate voltage as [18]

$$\hat{Q}_j = 2e\left(\hat{n}_j - n_{\mathrm{g},j}\right). \tag{3.37}$$

The flux ϕ_j is also promoted into operator $\hat{\phi}_j$ and it can be written with the help of the phase difference operator as [24]

$$\hat{\phi}_j = \Phi_0 \hat{\delta}_j/(2\pi). \tag{3.38}$$

Inserting Eqs. (3.37) and (3.38) in the qubit Hamiltonian (3.17) provides us with the CPB Hamiltonian

$$\begin{aligned}
\hat{\mathcal{H}}_{\mathrm{q},j} &= \frac{\hat{Q}_j^2}{2C_{\Sigma,j}} - E_{\mathrm{J},j}\cos\left(\frac{2\pi}{\Phi_0}\hat{\phi}_j\right) \\
&= \frac{(2e)^2}{2C_{\Sigma,j}}\left(\hat{n}_j - n_{\mathrm{g},j}\right)^2 - E_{\mathrm{J},j}\cos\left(\hat{\delta}_j\right) \\
&= 4E_{\mathrm{C},j}\left(\hat{n}_j - n_{\mathrm{g},j}\right)^2 - \frac{E_{\mathrm{J},j}}{2}\sum_n \left(|n+1\rangle_{j\,j}\langle n| + |n\rangle_{j\,j}\langle n+1|\right),
\end{aligned} \tag{3.39}$$

where we have defined the charging energy as $E_{\mathrm{C},j} = e^2/(2C_{\Sigma,j})$.

We assume that the CPB is operated in such a parameter regime that the number of excess Cooper pairs on the island is limited to two values, 0 and 1. This is the case if $0 < n_{\mathrm{g},j} < 1$ and $E_{\mathrm{C},j} \gg E_{\mathrm{J},j}$ [18]. Thus, the jth qubit can be analyzed as a two-level system with states $|0\rangle_j$ and $|1\rangle_j$ acting as eigenstates of $\hat{n}_j$ with eigenvalues 0 and 1, respectively. Here, the number operator for the excess Cooper pairs on the island reduces to

$$\hat{n}_j = \sum_n n\,|n\rangle_{j\,j}\langle n| = |1\rangle_{j\,j}\langle 1|. \tag{3.40}$$

We diagonalize the Hamiltonian (3.39) in this truncated basis, and as a result, obtain the eigenvectors

$$|\uparrow\rangle_j = \cos\left(\frac{\vartheta}{2}\right)|1\rangle_j - \sin\left(\frac{\vartheta}{2}\right)|0\rangle_j\,, \tag{3.41}$$

$$|\downarrow\rangle_j = \sin\left(\frac{\vartheta}{2}\right)|1\rangle_j + \cos\left(\frac{\vartheta}{2}\right)|0\rangle_j\,, \tag{3.42}$$

where the mixing angle ϑ is defined as

$$\cos\vartheta = \frac{4E_{\mathrm{C},j}(1-2n_{\mathrm{g},j})}{\sqrt{16E_{\mathrm{C},j}^2(1-2n_{\mathrm{g},j})^2 + E_{\mathrm{J},j}^2}}. \tag{3.43}$$

The energy eigenvalues are

$$E_j^{\pm} = \pm\frac{1}{2}\sqrt{16E_{\mathrm{C},j}^2(1-2n_{\mathrm{g},j})^2 + E_{\mathrm{J},j}^2}, \tag{3.44}$$

with E_j^+ and E_j^- corresponding to states $|\uparrow\rangle_j$ and $|\downarrow\rangle_j$, respectively. Here, we have shifted the zero point of the energy, since the interest lies in the energy difference of the eigenstates. Assuming that the bias voltage $V_{\mathrm{g},j}$ is tuned such that the normalized gate voltage becomes $n_{\mathrm{g},j} = 1/2$, we observe that $|\cos(\vartheta/2)|^2 = |\sin(\vartheta/2)|^2 = 1/2$. By evaluating the energy eigenstates in Eqs. (3.41) and (3.42) with these values, we note that there is an equal probability of finding one or zero excess Cooper pairs on the superconducting island. Furthermore, the eigenenergies become $E_j^{\pm} = \pm E_{\mathrm{J},j}/2$.

We can denote the energy difference between the eigenstates of the jth qubit by $\hbar\Omega_j$, where Ω_j is the transition frequency of the qubit. By definition, the qubit Hamiltonian (3.39) becomes diagonal in the energy eigenbasis. In the two-level approximation, it can be written in the form

$$\begin{aligned}\hat{\mathcal{H}}_{\mathrm{q},j} &\approx E_j^+\,|\uparrow\rangle_{j\,j}\langle\uparrow| + E_j^-\,|\downarrow\rangle_{j\,j}\langle\downarrow| \\ &= \frac{\hbar}{2}\Omega_j\hat{\sigma}_j^z,\end{aligned} \tag{3.45}$$

where $\hat{\sigma}_j^z = |\uparrow\rangle_{j\,j}\langle\uparrow| - |\downarrow\rangle_{j\,j}\langle\downarrow|$. Furthermore, by shifting the zero point of the energy by E_j^-, the Hamiltonian can be expressed as

$$\hat{\mathcal{H}}_{\mathrm{q},j} \approx 2E_j^+ \, |\uparrow\rangle_{j\,j}\langle\uparrow| = \hbar\Omega_j \hat{\sigma}_j^+ \hat{\sigma}_j^- , \tag{3.46}$$

where $\hat{\sigma}_j^+ = |\uparrow\rangle_{j\,j}\langle\downarrow|$ and $\hat{\sigma}_j^- = \left(\hat{\sigma}_j^+\right)^\dagger$. Assuming $n_{\mathrm{g},j} = 1/2$, we may present the charge operator of Eq. (3.37) in terms of the qubit energy eigenstates as

$$\begin{aligned} \hat{Q}_j &= 2e\left(|1\rangle_{j\,j}\langle 1| - \frac{1}{2}\right) \\ &= e\left(\hat{\sigma}_j^+ + \hat{\sigma}_j^-\right). \end{aligned} \tag{3.47}$$

3.3.3 Transmon regime

For a moderately large ratio of $E_{\mathrm{J},j}/E_{\mathrm{C},j}$, corresponding to the transmon regime in this design of the superconducting qubit, the states of the superconducting island cannot be approximated with only two charge states [19]. Therefore, the above considerations corresponding to the CPB are not valid as such. Moreover, the energy levels for the transmon qubit are very insensitive to the normalized gate voltage $n_{\mathrm{g},j}$, and hence it is not included here. In the transmon case, the Hamiltonian can be approximated as a harmonic oscillator with a quartic perturbation [19]

$$\hat{\mathcal{H}}_{\mathrm{q},j} \approx \sqrt{8E_{\mathrm{C},j}E_{\mathrm{J},j}}\left(\hat{b}^\dagger\hat{b} + \frac{1}{2}\right) - E_{\mathrm{J},j} - \frac{E_{\mathrm{C},j}}{12}\left(\hat{b} + \hat{b}^\dagger\right)^4, \tag{3.48}$$

where $\hat{b}$ and $\hat{b}^\dagger$ are the annihilation and creation operators, respectively, for the approximated harmonic oscillator. The energy levels are approximated as the eigenenergies of the harmonic oscillator with a perturbation term arising from the quartic term [19]

$$E_m \approx -E_{\mathrm{J},j} + \sqrt{8E_{\mathrm{C},j}E_{\mathrm{J},j}}\left(m + \frac{1}{2}\right) - \frac{E_{\mathrm{C},j}}{12}\left(6m^2 + 6m + 3\right). \tag{3.49}$$

The anharmonicity in the energy levels justifies the two-level approximation for the transmon qubit.

3.3.4 Coupling term

Within the narrow-bandwidth approximation for the transmission line charge density operator $\hat{q}(x)$ of Eq. (3.35), the two-level system approximation for

the qubit charge operator $\hat{Q}_j$ of Eq. (3.47), and $n_{\mathrm{g},j} = 1/2$, the coupling term of the jth qubit in the Schrödinger picture assumes the form

$$\begin{aligned}\hat{\mathcal{H}}_{\mathrm{c},j} &= \frac{\hat{Q}_j \hat{q}(x)}{c_{\mathrm{c},j}} \\ &\approx \hbar V_j \int_0^\infty d\omega \left[\hat{a}_{\mathrm{L}}(\omega) e^{-i\omega x_j/v} + \hat{a}_{\mathrm{R}}(\omega) e^{i\omega x_j/v} + \mathrm{h.c.}\right] \left(\hat{\sigma}_j^+ + \hat{\sigma}_j^-\right), \quad (3.50)\end{aligned}$$

where the coupling constant V_j depends on the type of the superconducting qubit. For the CPB, direct calculation shows that the coupling constant is given by

$$V_{j,\mathrm{CPB}} = \frac{ce}{c_{\mathrm{c},j}} \sqrt{\frac{Z_0 \omega_0}{4\pi\hbar}}. \quad (3.51)$$

The coupling coefficient V_j in the coupling Hamiltonian (3.50) for the transmon qubit becomes [23]

$$V_{j,\mathrm{transmon}} \approx \frac{ce}{c_{\mathrm{c},j}} \sqrt{\frac{Z_0 \omega_0}{4\pi\hbar}} \left(\frac{E_{\mathrm{J},j}}{2E_{\mathrm{C},j}}\right)^{1/4}. \quad (3.52)$$

3.4 Real-space Hamiltonian

In this section, we present the Hamiltonian (3.15) in terms of the field operators of the photons. The creation and annihilation operators for the photons can be written as Fourier transforms of the field operators

$$\hat{a}_{\mathrm{R/L}}(\omega) = \frac{1}{\sqrt{2\pi v}} \int_{-\infty}^{\infty} dx\, \hat{a}_{\mathrm{R/L}}(x) e^{\mp i\omega x/v}, \quad (3.53)$$

$$\hat{a}_{\mathrm{R/L}}^\dagger(\omega) = \frac{1}{\sqrt{2\pi v}} \int_{-\infty}^{\infty} dx\, \hat{a}_{\mathrm{R/L}}^\dagger(x) e^{\pm i\omega x/v}, \quad (3.54)$$

where $\hat{a}_\alpha^\dagger(x)$ and $\hat{a}_\alpha(x)$ create and annihilate a photon moving in the $\alpha \in \{\mathrm{R}, \mathrm{L}\}$ direction at position x, respectively. The definition of $\hat{a}_\alpha(x)$ is given in Eq. (3.34) and its Hermitian conjugate defines $\hat{a}_\alpha^\dagger(x)$. The first term in

the transmission line Hamiltonian (3.30) becomes

$$\begin{aligned}\int_0^\infty d\omega\,\hbar\omega\hat{a}_{\mathrm{R}}^\dagger(\omega)\hat{a}_{\mathrm{R}}(\omega) &\approx \int_{-\infty}^\infty d\omega\,\hbar\omega\hat{a}_{\mathrm{R}}^\dagger(\omega)\hat{a}_{\mathrm{R}}(\omega)\\ &= \int_{-\infty}^\infty d\omega\,\hbar\omega\int_{-\infty}^\infty dx\int_{-\infty}^\infty dx'\hat{a}_{\mathrm{R}}^\dagger(x)\hat{a}_{\mathrm{R}}(x')\frac{1}{2\pi v}e^{i\omega(x-x')/v}\\ &= i\hbar v\int_{-\infty}^\infty dx\int_{-\infty}^\infty dx'\hat{a}_{\mathrm{R}}^\dagger(x)\hat{a}_{\mathrm{R}}(x')\frac{d}{dx'}\delta(x-x')\\ &= -i\hbar v\int_{-\infty}^\infty dx\,\hat{a}_{\mathrm{R}}^\dagger(x)\frac{d}{dx}\hat{a}_{\mathrm{R}}(x). \end{aligned} \tag{3.55}$$

The integration limits can be extended from $[0,\infty)$ to $(-\infty,\infty)$, since we are working within a narrow bandwidth of frequencies. Thus, the contribution from the negative frequencies will be zero [27]. On the third line, we have used the change of variables and the definition of the Dirac delta function as

$$\begin{aligned}\frac{1}{2\pi}\int_{-\infty}^\infty d\omega\,\omega e^{i\omega(x-x')/v} &= \frac{v^2}{2\pi}\int_{-\infty}^\infty dk\,ke^{ik(x-x')}\\ &= \frac{v^2}{2\pi}\int_{-\infty}^\infty dk\,k\frac{1}{-ik}\frac{d}{dx'}e^{ik(x-x')}\\ &= i\frac{v^2}{2\pi}\frac{d}{dx'}\left(\int_{-\infty}^\infty dk\,e^{ik(x-x')}\right)\\ &= iv^2\frac{d}{dx'}\delta(x-x'). \end{aligned} \tag{3.56}$$

On the fourth line we assume $\lim_{x\to\pm\infty}\hat{a}_{\mathrm{R}}(x) = \lim_{x\to\pm\infty}\hat{a}_{\mathrm{R}}^\dagger(x) = 0$, and integrate by parts as

$$\begin{aligned} iv\hbar&\int_{-\infty}^\infty dx\int_{-\infty}^\infty dx'\,\hat{a}_{\mathrm{R}}^\dagger(x)\hat{a}_{\mathrm{R}}(x')\frac{d}{dx'}\delta(x-x')\\ &= iv\hbar\int_{-\infty}^\infty dx\int_{-\infty}^\infty dx'\,\hat{a}_{\mathrm{R}}^\dagger(x)\left\{\frac{d}{dx'}\left[\hat{a}_{\mathrm{R}}(x')\delta(x-x')\right]\right.\\ &\qquad\left.-\delta(x-x')\frac{d}{dx'}\hat{a}_{\mathrm{R}}(x')\right\}\\ &= -iv\hbar\int_{-\infty}^\infty dx\int_{-\infty}^\infty dx'\,\hat{a}_{\mathrm{R}}^\dagger(x)\delta(x-x')\frac{d}{dx'}\hat{a}_{\mathrm{R}}(x')\\ &= -iv\hbar\int_{-\infty}^\infty dx\,\hat{a}_{\mathrm{R}}^\dagger(x)\frac{d}{dx}\hat{a}_{\mathrm{R}}(x). \end{aligned} \tag{3.57}$$

Similarly, the second term in the transmission line Hamiltonian (3.30) becomes

$$\int_0^\infty d\omega\,\hbar\omega\hat{a}_{\mathrm{L}}^\dagger(\omega)\hat{a}_{\mathrm{L}}(\omega) \approx iv\hbar\int_{-\infty}^\infty dx\,\hat{a}_{\mathrm{L}}^\dagger(x)\frac{d}{dx}\hat{a}_{\mathrm{L}}(x). \tag{3.58}$$

Below, we employ the rotating wave approximation (RWA) on the coupling Hamiltonian (3.50), i.e., we drop the terms proportional to $\hat{a}_\alpha(x)\hat{\sigma}_-$ or $\hat{a}^\dagger_\alpha(x)\hat{\sigma}_+$. This approximation is valid if the photon frequency is nearly resonant with the transition frequencies of the qubits, i.e., $|\Omega_j - \omega| \ll \Omega_j + \omega$ $\forall j$. The removed terms are quickly oscillating in the interaction picture (see Sec. 2.4.1) and their contribution to the temporal evolution of the system averages out in the relevant time scales. Furthermore, we again assume that we are working with a narrow bandwidth of frequencies, allowing us to extend the integration limits. Within these approximations, the coupling Hamiltonian (3.50) assumes the form

$$\begin{aligned}
\hat{\mathcal{H}}_{\mathrm{c},j} &\approx \hbar V_j \int_{-\infty}^{\infty} d\omega \Big[\hat{a}_{\mathrm{L}}(\omega) e^{-i\omega x_j/v} \hat{\sigma}_j^+ + \hat{a}_{\mathrm{R}}(\omega) e^{i\omega x_j/v} \hat{\sigma}_j^+ \\
&\quad + \hat{a}^\dagger_{\mathrm{L}}(\omega) e^{i\omega x_j/v} \hat{\sigma}_j^- + \hat{a}^\dagger_{\mathrm{R}}(\omega) e^{-i\omega x_j/v} \hat{\sigma}_j^- \Big] \\
&= \hbar V_j \sqrt{\frac{1}{2\pi v}} \int_{-\infty}^{\infty} d\omega \int_{-\infty}^{\infty} dx \Big[\hat{a}_{\mathrm{L}}(x) e^{-i\omega(x_j - x)/v} \hat{\sigma}_j^+ + \hat{a}_{\mathrm{R}}(x) e^{-i\omega(x - x_j)/v} \hat{\sigma}_j^+ \\
&\quad + \hat{a}^\dagger_{\mathrm{L}}(x) e^{-i\omega(x - x_j)/v} \hat{\sigma}_j^- + \hat{a}^\dagger_{\mathrm{R}}(x) e^{-i\omega(x_j - x)/v} \hat{\sigma}_j^- \Big] \\
&= \hbar g_j \int_{-\infty}^{\infty} dx\, \delta(x - x_j) \left[\hat{a}^\dagger_{\mathrm{R}}(x) \hat{\sigma}_j^- + \hat{a}_{\mathrm{R}}(x) \hat{\sigma}_j^+ + \hat{a}^\dagger_{\mathrm{L}}(x) \hat{\sigma}_j^- + \hat{a}_{\mathrm{L}}(x) \hat{\sigma}_j^+ \right] \\
&= \hbar g_j \left[\hat{a}^\dagger_{\mathrm{R}}(x_j) \hat{\sigma}_j^- + \hat{a}_{\mathrm{R}}(x_j) \hat{\sigma}_j^+ + \hat{a}^\dagger_{\mathrm{L}}(x_j) \hat{\sigma}_j^- + \hat{a}_{\mathrm{L}}(x_j) \hat{\sigma}_j^+ \right], \qquad (3.59)
\end{aligned}$$

where the coupling constant is given by $g_j = V_j \sqrt{2\pi v}$. Finally, the quantized Hamiltonian describing the circuit within the RWA, the narrow-bandwidth, and the two-level approximation, is written with the help of the field operators as

$$\hat{\mathcal{H}} = \hat{\mathcal{H}}_{\mathrm{TL}} + \sum_{j=0}^{N-1} \left(\hat{\mathcal{H}}_{\mathrm{q},j} + \hat{\mathcal{H}}_{\mathrm{c},j} \right), \qquad (3.60)$$

$$\hat{\mathcal{H}}_{\mathrm{TL}} \approx -iv\hbar \int_{-\infty}^{\infty} dx \left[\hat{a}^\dagger_{\mathrm{R}}(x) \frac{d}{dx} \hat{a}_{\mathrm{R}}(x) - \hat{a}^\dagger_{\mathrm{L}}(x) \frac{d}{dx} \hat{a}_{\mathrm{L}}(x) \right], \qquad (3.61)$$

$$\hat{\mathcal{H}}_{\mathrm{q},j} \approx \hbar \Omega_j \hat{\sigma}_j^+ \hat{\sigma}_j^-, \qquad (3.62)$$

$$\hat{\mathcal{H}}_{\mathrm{c},j} \approx \hbar g_j \left[\hat{a}^\dagger_{\mathrm{R}}(x_j) \hat{\sigma}_j^- + \hat{a}_{\mathrm{R}}(x_j) \hat{\sigma}_j^+ + \hat{a}^\dagger_{\mathrm{L}}(x_j) \hat{\sigma}_j^- + \hat{a}_{\mathrm{L}}(x_j) \hat{\sigma}_j^+ \right]. \qquad (3.63)$$

The resulting Hamiltonian has the same form as the Hamiltonian describing a general waveguide to which two-level systems are coupled [28, 29]. Dissipation may be modeled by coupling the system to an external reservoir. In practice, the simplest approximative way to take dissipation into account is

to add the following term into the Hamiltonian [29, 30]:

$$\hat{\mathcal{H}}_{\text{diss}} = -\frac{i}{2}\sum_{j=0}^{N-1}\Gamma'_j\hat{\sigma}_j^+\hat{\sigma}_j^-, \tag{3.64}$$

where Γ'_j is the decay rate of the jth qubit due to its reservoir.

Chapter 4

Methods: few-photon scattering

In this chapter, we calculate the scattering properties of a single-photon input state in a superconducting transmission line with symmetric coupling to one or three superconducting qubits. Furthermore, by following the technique presented in Ref. [29], we calculate the scattering eigenstate for the two-photon input and the corresponding two-photon wavefunction.

4.1 Single-photon scattering

4.1.1 Scattering from a single qubit

Let us consider a system in which a single qubit with transition frequency Ω is coupled to a transmission line at $x = 0$ with coupling strength $g_1 = g$, and a single photon with energy $E = \hbar v k$ is initially travelling in the $\alpha \in \{\mathrm{R}, \mathrm{L}\}$ direction. This system is modeled by the Hamiltonian (3.60) with $N = 1$ and $x_0 = 0$. Since the Hamiltonian (3.60) is derived within the RWA, it preserves the number of excitations in the system. The single-excitation eigenstate $|\phi_1(k); \alpha\rangle$, for which $\hat{\mathcal{H}} |\phi_1(k); \alpha\rangle = \hbar v k |\phi_1(k); \alpha\rangle$, is written as [29]

$$|\phi_1(k); \alpha\rangle = \left\{ \int dx \left[\phi^{\alpha}_{\mathrm{R}}(k, x) \hat{a}^{\dagger}_{\mathrm{R}}(x) + \phi^{\alpha}_{\mathrm{L}}(k, x) \hat{a}^{\dagger}_{\mathrm{L}}(x) \right] + e^{\alpha}(k) \hat{\sigma}^{+}_{1} \right\} |0; \mathrm{g}\rangle \,, \quad (4.1)$$

where the $\phi^{\alpha}_{\alpha'}(k, x)$ is the single-photon wavefunction for a photon traveling in the α' direction with the initial direction of α, and $e^{\alpha}(k)$ is the amplitude associated with the probability of finding the qubit in the excited state. The vacuum state is given by $|0; \mathrm{g}\rangle$, where the digit denotes the number of photons in the waveguide and the letter denotes that the two-level system is in the ground state. It turns out that plane-wave solutions are sufficient for this

problem, and we can write [29]

$$\phi_{\mathrm{R}}^{\mathrm{R}}(k,x) = \frac{e^{ikx}}{\sqrt{2\pi}}\left[\theta(-x) + t_1^{\mathrm{R}}(k)\theta(x)\right], \tag{4.2}$$

$$\phi_{\mathrm{L}}^{\mathrm{R}}(k,x) = \frac{e^{-ikx}}{\sqrt{2\pi}} r_1^{\mathrm{R}}(k)\theta(-x), \tag{4.3}$$

$$\phi_{\mathrm{R}}^{\mathrm{L}}(k,x) = \frac{e^{ikx}}{\sqrt{2\pi}} r_1^{\mathrm{L}}(k)\theta(x), \tag{4.4}$$

$$\phi_{\mathrm{L}}^{\mathrm{L}}(k,x) = \frac{e^{-ikx}}{\sqrt{2\pi}}\left[t_1^{\mathrm{L}}(k)\theta(-x) + \theta(x)\right], \tag{4.5}$$

where $\Theta(x)$ the Heaviside step function defined as

$$\Theta(x) = \begin{cases} 0, & x < 0 \\ 1, & x > 0 \\ \frac{1}{2}, & x = 0. \end{cases} \tag{4.6}$$

The coefficients $t_1^{\alpha}(k)$ and $r_1^{\alpha}(k)$ are the transmission and reflection coefficients, respectively, for a photon propagating initially in the α direction [31]. The Schrödinger equation provides the following solutions for the amplitudes (see Appendix A for derivation)

$$t_1^{\mathrm{R}}(k) = t_1^{\mathrm{L}}(k) = \frac{1}{1 + i\Gamma/\left[\sqrt{2\pi}(2vk - 2\Omega)\right]}, \tag{4.7}$$

$$r_1^{\mathrm{R}}(k) = r_1^{\mathrm{L}}(k) = -\frac{\Gamma}{\Gamma - 2i\sqrt{2\pi}(vk - \Omega)}, \tag{4.8}$$

$$e_1^{\mathrm{R}}(k) = e_1^{\mathrm{L}}(k) = -\frac{2ig}{\Gamma - 2i\sqrt{2\pi}(vk - \Omega)}, \tag{4.9}$$

where Γ is the decay rate as defined in Appendix A. For the CPB qubit, the coupling strength V_{CPB} is defined in Eq. (3.51) and for the transmon qubit in Eq. (3.52). The decay rates for the CPB and transmon qubits assume the forms

$$\Gamma_{\mathrm{CPB}} = 4\pi V_{\mathrm{CPB}}^2 = \frac{c^2 e^2 Z_0 \omega_0}{\hbar c_{\mathrm{c}}^2}, \tag{4.10}$$

$$\Gamma_{\mathrm{transmon}} = 4\pi V_{\mathrm{transmon}}^2 = \frac{c^2 e^2 Z_0 \omega_0}{\hbar c_{\mathrm{c}}^2}\sqrt{\frac{E_{\mathrm{J}}}{2E_{\mathrm{C}}}}. \tag{4.11}$$

4.1.2 Scattering from three qubits

We investigate the case of symmetrically coupled three superconducting qubits by extending the formalism of Ref. [29]. Here, we employ the Hamiltonian (3.60) and set $N = 3$, $x_0 = -L$, $x_1 = 0$, and $x_2 = L$. Assuming a

photon traveling initially in the α direction, the single-photon eigenstate is given by

$$|\phi_1(k);\alpha\rangle = \Bigg\{ \int dx \left[\phi_{\mathrm{R}}^{\alpha}(k,x)\hat{a}_{\mathrm{R}}^{\dagger}(x) + \phi_{\mathrm{L}}^{\alpha}(k,x)\hat{a}_{\mathrm{L}}^{\dagger}(x)\right] + e_1^{\alpha}(k)\hat{\sigma}_1^{+} + e_2^{\alpha}(k)\hat{\sigma}_2^{+} + e_3^{\alpha}(k)\hat{\sigma}_3^{+} \Bigg\} |0;\mathrm{ggg}\rangle\,, \tag{4.12}$$

where $|0;\mathrm{ggg}\rangle$ is the vacuum state with zero photons in the waveguide and all three qubits in their respective ground states. The wavefunctions are given by

$$\begin{aligned}
\phi_{\mathrm{R}}^{\mathrm{R}}(k,x) &= \frac{e^{ikx}}{\sqrt{2\pi}}\left[\theta(-L-x) + t_{12}^{\mathrm{R}}(k)\theta(x+L)\theta(-x)\right. \\
&\quad \left. + t_{23}^{\mathrm{R}}(k)\theta(x)\theta(L-x) + t_{3}^{\mathrm{R}}(k)\theta(x-L)\right], \qquad (4.13)\\
\phi_{\mathrm{L}}^{\mathrm{R}}(k,x) &= \frac{e^{-ikx}}{\sqrt{2\pi}}\left[r_{3}^{\mathrm{R}}(k)\theta(-L-x) + r_{12}^{\mathrm{R}}(k)\theta(x+L)\theta(-x)\right. \\
&\quad \left. + r_{23}^{\mathrm{R}}(k)\theta(x)\theta(L-x)\right], \qquad (4.14)\\
\phi_{\mathrm{R}}^{\mathrm{L}}(k,x) &= \frac{e^{ikx}}{\sqrt{2\pi}}\left[r_{12}^{\mathrm{L}}(k)\theta(x+L)\theta(-x) + r_{23}^{\mathrm{L}}(k)\theta(x)\theta(L-x)\right. \\
&\quad \left. + r_{3}^{\mathrm{L}}(k)\theta(x-L)\right], \qquad (4.15)\\
\phi_{\mathrm{L}}^{\mathrm{L}}(k,x) &= \frac{e^{-ikx}}{\sqrt{2\pi}}\left[t_{3}^{\mathrm{L}}(k)\theta(-L-x) + t_{12}^{\mathrm{L}}(k)\theta(x+L)\theta(-x)\right. \\
&\quad \left. + t_{23}^{\mathrm{L}}(k)\theta(x)\theta(L-x) + \theta(x-L)\right]. \qquad (4.16)
\end{aligned}$$

Furthermore, we introduce the decay rates $\Gamma_i = 2g_i^2/v$, and assume $\Gamma_1 = \Gamma_3 \equiv \Gamma$, $\Gamma_2 = \gamma\Gamma$, as well as $\Omega_1 = \Omega_2 = \Omega_3 \equiv \Omega$ to preserve symmetry. Consequently, we obtain the following lengthy solutions from the Schrödinger equation:

$$t_3^{\mathrm{R}}(k) = t_3^{\mathrm{L}}(k) = \frac{8i\delta^3}{\gamma\Gamma\left[2i\delta + \Gamma\left(-1+e^{ikL}\right)\right]^2 + 2i\delta\left[(2\delta+i\Gamma)^2 + \Gamma^2 e^{2ikL}\right]}, \tag{4.17}$$

$$t_{12}^{\mathrm{R}}(k) = t_{23}^{\mathrm{L}}(k) = \frac{2i\delta\left[(2\delta+i\Gamma)(2\delta+i\gamma\Gamma) + \gamma\Gamma^2 e^{ikL}\right]}{\gamma\Gamma\left[2i\delta + \Gamma\left(-1+e^{ikL}\right)\right]^2 + 2i\delta\left[(2\delta+i\Gamma)^2 + \Gamma^2 e^{2ikL}\right]}, \tag{4.18}$$

$$t_{23}^{\mathrm{R}}(k) = t_{12}^{\mathrm{L}}(k) = -\frac{4\delta^2(\Gamma-2i\delta)}{\gamma\Gamma\left[2i\delta + \Gamma\left(-1+e^{ikL}\right)\right]^2 + 2i\delta\left[(2\delta+i\Gamma)^2 + \Gamma^2 e^{2ikL}\right]}, \tag{4.19}$$

$$r_3^{\mathrm{R}}(k) = r_3^{\mathrm{L}}(k) = \frac{\Gamma e^{-2ikL}\left[(\Gamma-2i\delta)(\gamma\Gamma-2i\delta) - 2\gamma\left(\Gamma^2+2\delta^2\right)e^{ikL} + (\Gamma+2i\delta)e^{2ikL}(\gamma\Gamma+2i\delta)\right]}{2\left[2\delta - i\Gamma\left(-1+e^{ikL}\right)\right]\left\{\gamma\Gamma^2 e^{\frac{1}{2}ikL}\sin(kL) + \delta\left[\Gamma\left(\gamma+e^{ikL}+1\right)-2i\delta\right]\right\}}, \tag{4.20}$$

$$r_{12}^{\mathrm{R}}(k) = r_{23}^{\mathrm{L}}(k) = \frac{2\Gamma\delta\left[e^{ikL}(\gamma\Gamma+2i\delta) - \gamma(\Gamma-2i\delta)\right]}{i\gamma\Gamma\left[2i\delta + \Gamma\left(-1+e^{ikL}\right)\right]^2 + 2\delta\left[(\Gamma-2i\delta)^2 - \Gamma^2 e^{2ikL}\right]}, \tag{4.21}$$

$$r_{23}^{\mathrm{R}}(k) = r_{12}^{\mathrm{L}}(k) = \frac{4\Gamma\delta^2 e^{ikL}}{\gamma\Gamma\left[2i\delta + \Gamma\left(-1+e^{ikL}\right)\right]^2 + 2i\delta\left[(2\delta+i\Gamma)^2 + \Gamma^2 e^{2ikL}\right]}, \tag{4.22}$$

$$e_1^{\mathrm{R}}(k) = e_3^{\mathrm{L}}(k) = \frac{2\sqrt{v\Gamma}e^{-\frac{1}{2}ikL}\left\{-\delta(\gamma\Gamma+\Gamma-2i\delta) + \gamma\Gamma e^{ikL}\left[\delta + 2i\Gamma\sin^2(kL)\right] + \Gamma\delta e^{2ikL}\right\}}{\sqrt{\pi}\left[2i\delta+\Gamma\left(-1+e^{ikL}\right)\right]\left[\Gamma e^{ikL}(\gamma\Gamma+2i\delta) - (\Gamma-2i\delta)(\gamma\Gamma-2i\delta)\right]}, \tag{4.23}$$

$$e_2^{\mathrm{R}}(k) = e_2^{\mathrm{L}}(k) = \frac{2\delta\sqrt{v\gamma\Gamma}}{\sqrt{\pi}\left[\Gamma e^{ikL}(\gamma\Gamma+2i\delta) - (\Gamma-2i\delta)(\gamma\Gamma-2i\delta)\right]}, \tag{4.24}$$

$$e_3^{\mathrm{R}}(k) = e_1^{\mathrm{L}}(k) = \frac{4i\delta^2\sqrt{v\Gamma}e^{\frac{1}{2}ikL}}{\sqrt{\pi}\left[2i\delta+\Gamma\left(-1+e^{ikL}\right)\right]\left[\Gamma e^{ikL}(\gamma\Gamma+2i\delta) - (\Gamma-2i\delta)(\gamma\Gamma-2i\delta)\right]}, \tag{4.25}$$

where we have defined the detuning $\delta = vk - \Omega$. Absolute value squared and phase of the transmission coefficient for different values of the coupling ratio γ are presented in Fig. 4.1. For small values of the coupling ratio γ, the transmission starts to resemble the case of two qubits which was studied in Ref. [29]. For large γ, the coupling in the middle qubit dominates, and the regime for full transmission is rather narrow.

4.2 Two-photon scattering

In this section, we focus on the scattering of two-photon input states by taking into account both linear and nonlinear effects. The nonlinearity arises from the effective interactions between two photons mediated by the two-level systems coupled to the waveguide. For a single two-level system coupled to

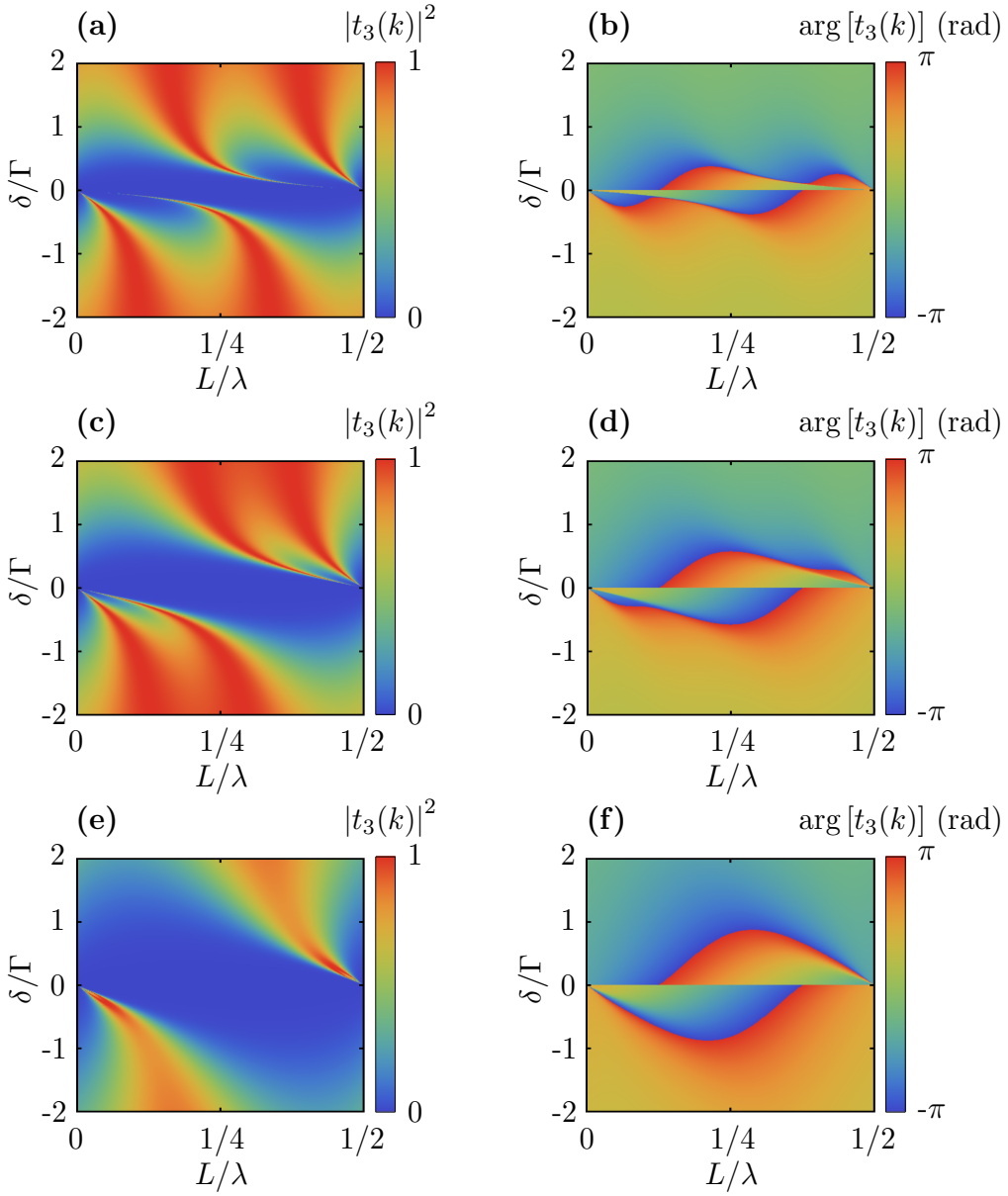

Figure 4.1: Absolute value squared, $|t_3(k)|^2$, and the phase, $\arg[t_3(k)]$, of the transmission coefficient as a function of distance between qubits, L, and the detuning between the qubit and photon frequencies, δ. The distance L is in the units of the wavelength of the photon $\lambda = 2\pi/k$, and the detuning is in the units of the decay rate of the side qubits $\Gamma = \Gamma_1 = \Gamma_3$. The coupling ratio $\gamma = \Gamma_2/\Gamma$ is set to (a), (b) $\gamma = 0.25$, (c), (d) $\gamma = 1$, and (e), (f) $\gamma = 4$.

an infinite waveguide, an analytical solution can be derived for the scattering eigenstates for an arbitrary number of photons [32].

However, for multi-photon scattering with arbitrary number of qubits, no analytical solution is known to exist. Instead, we review the Green's function method presented in Ref. [29] and employ it in the calculations. In this approach, we first treat the qubits as bosonic sites, i.e., we set $\hat{\sigma}_j^- \to \hat{d}_j$ and $\hat{\sigma}_j^+ \to \hat{d}_j^\dagger$, where the creation and annihilation operators for the bosonic sites $\hat{d}_j^\dagger$ and $\hat{d}_j$ satisfy the usual commutation relations. The terms in the Hamiltonian (3.60) transform as $\hat{\mathcal{H}}_{\mathrm{q},j} \to \hat{\mathcal{H}}^{\mathrm{b}}_{\mathrm{q},j}$ and $\hat{\mathcal{H}}_{\mathrm{int},j} \to \hat{\mathcal{H}}^{\mathrm{b}}_{\mathrm{int},j}$, where

$$\hat{\mathcal{H}}^{\mathrm{b}}_{\mathrm{q},j} = \hbar\Omega_j \hat{d}_j^\dagger \hat{d}_j, \tag{4.26}$$

$$\hat{\mathcal{H}}^{\mathrm{b}}_{\mathrm{int},j} = \hbar g_j \left[\hat{a}^\dagger_{\mathrm{R}}(x_j)\hat{d}_j + \hat{a}_{\mathrm{R}}(x_j)\hat{d}_j^\dagger + \hat{a}^\dagger_{\mathrm{L}}(x_j)\hat{d}_j + \hat{a}_{\mathrm{L}}(x_j)\hat{d}_j^\dagger\right]. \tag{4.27}$$

The transmission line Hamiltonian $\hat{\mathcal{H}}_{\mathrm{TL}}$ is not affected. This transformation allows, in principle, multiple occupancies in the qubit sites, but population in the high-lying states is eventually prohibited by the introduction of an interaction term $\hat{\mathcal{V}}_j$ for each qubit. The interaction terms read

$$\hat{\mathcal{V}}_j \equiv \frac{U}{2}\hat{d}_j^\dagger \hat{d}_j(\hat{d}_j^\dagger \hat{d}_j - 1), \tag{4.28}$$

where U is the interaction strength. This term is nonzero only for sites with multiple occupancies. In the end, we take the limit $U \to \infty$. Thus no site may have occupation greater than unity in the scattering eigenstate, since it would require an infinite amount of energy in this limit.

With these additions, the Hamiltonian may be expressed as

$$\hat{\mathcal{H}}^{\mathrm{b}} = \hat{\mathcal{H}}_0 + \sum_{j=0}^{N-1} \hat{\mathcal{V}}_j, \tag{4.29}$$

where the noninteracting part is defined as

$$\hat{\mathcal{H}}_0 \equiv \hat{\mathcal{H}}_{\mathrm{TL}} + \sum_{j=0}^{N-1} \left(\hat{\mathcal{H}}^{\mathrm{b}}_{\mathrm{q},j} + \hat{\mathcal{H}}^{\mathrm{b}}_{\mathrm{int},j}\right). \tag{4.30}$$

The single-excitation eigenstate for the Hamiltonian $\hat{\mathcal{H}}_0$ is given by

$$|\phi_1(k);\alpha\rangle = \left\{ \int dx \left[\phi^\alpha_{\mathrm{R}}(k,x)\hat{a}^\dagger_{\mathrm{R}}(x) + \phi^\alpha_{\mathrm{L}}(k,x)\hat{a}^\dagger_{\mathrm{L}}(x)\right] + \sum_{j=0}^{N-1} e_j^\alpha(k)\hat{d}_j^\dagger \right\} |0;\mathbf{0}\rangle, \tag{4.31}$$

where $|0;\mathbf{0}\rangle = |0;00...0\rangle$ is the vacuum state, where the first digit corresponds to the number of photons in the waveguide, and the vector of digits after the semicolon indicates the number of bosons in the bosonic sites. In the vacuum state, there are zero photons in the waveguide and occupations are zero for each site. The evaluation of the wavefunctions $\phi_\alpha^{\alpha'}(k,x)$ and amplitudes $e_j^\alpha(k)$ is carried out as in Appendix A with the two-level systems, i.e., the results for the single-qubit case [Eqs. (4.7)–(4.9)] and for the three-qubit case [Eqs. (4.17)–(4.25)] are valid as such.

The noninteracting two-photon eigenstates $|\phi_2(k_1,k_2);\alpha_1,\alpha_2\rangle$ are direct products of single-photon states [29]

$$\begin{aligned}
|\phi_2(k_1,k_2);\alpha_1,\alpha_2\rangle &= |\phi_1(k_1);\alpha_1\rangle \otimes |\phi_1(k_2);\alpha_2\rangle \\
&= \Bigg\{ \int dx_1 \int dx_2 \sum_{\alpha_1',\alpha_2'} \phi_{\alpha_1'}^{\alpha_1}(k_1,x_1)\phi_{\alpha_2'}^{\alpha_2}(k_2,x_2)\hat{a}_{\alpha_1'}^\dagger(x_1)\hat{a}_{\alpha_2'}^\dagger(x_2) \\
&\quad + \int dx \sum_{\alpha_1',j} \phi_{\alpha_1'}^{\alpha_1}(k_1,x)e_j^{\alpha_2}(k_2)\hat{a}_{\alpha_1'}^\dagger(x)\hat{d}_j^\dagger \\
&\quad + \int dx \sum_{\alpha_2',j} \phi_{\alpha_2'}^{\alpha_2}(k_2,x)e_j^{\alpha_1}(k_1)\hat{a}_{\alpha_2'}^\dagger(x)\hat{d}_j^\dagger \\
&\quad + \sum_{j,j'} e_j^{\alpha_1}(k_1)e_{j'}^{\alpha_2}(k_2)\hat{d}_j^\dagger\hat{d}_j^\dagger \Bigg\} |0;\mathbf{0}\rangle \,. \qquad (4.32)
\end{aligned}$$

The above state is symmetrized by writing

$$\begin{aligned}
&\phi_{\alpha_1'}^{\alpha_1}(k_1,x_1)\phi_{\alpha_2'}^{\alpha_2}(k_2,x_2)\hat{a}_{\alpha_1'}^\dagger(x_1)\hat{a}_{\alpha_2'}^\dagger(x_2) \\
&\quad \to \frac{1}{2}\Big[\phi_{\alpha_1'}^{\alpha_1}(k_1,x_1)\phi_{\alpha_2'}^{\alpha_2}(k_2,x_2)\hat{a}_{\alpha_1'}^\dagger(x_1)\hat{a}_{\alpha_2'}^\dagger(x_2) + (1 \leftrightarrow 2)\Big], \qquad (4.33) \\
&e_j^{\alpha_1}(k_1)e_j^{\alpha_2}(k_2)\hat{d}_j^\dagger\hat{d}_j^\dagger \to \frac{1}{\sqrt{2}}e_j^{\alpha_1}(k_1)e_j^{\alpha_2}(k_2)\hat{d}_j^\dagger\hat{d}_j^\dagger, \qquad (4.34)
\end{aligned}$$

where $(1 \leftrightarrow 2)$ refers to the previous expression within the brackets with the index of x changed.

The noninteracting state $|\phi_2(k_1,k_2);\alpha_1,\alpha_2\rangle$ has a continuous energy spectrum with $E = \hbar v(k_1+k_2)$ [29]. We assume that this state interacts with a scattering potential defined by Eq. (4.28). The scattered state, namely $|\psi_2(k_1,k_2);\alpha_1,\alpha_2\rangle$, is calculated by examining the Lippmann–Schwinger (LS)

equation [29, 33, 34]

$$|\psi_2(k_1,k_2);\alpha_1,\alpha_2\rangle = |\phi_2(k_1,k_2);\alpha_1,\alpha_2\rangle + \hat{G}(E)\sum_{j=0}^{N-1}\hat{\mathcal{V}}_j\,|\psi_2(k_1,k_2);\alpha_1,\alpha_2\rangle\,, \tag{4.35}$$

where we have defined the Green's function

$$\hat{G}(E) \equiv \frac{1}{E-\hat{\mathcal{H}}_0+i\epsilon}. \tag{4.36}$$

The non-physical constant $\epsilon > 0$ is introduced here to enable contour integration techniques. Furthermore, its sign determines whether the obtained solutions are outgoing (plus) or incoming (minus) fields [33]. At the end of the calculations, we take the limit $\epsilon \to 0$.

In order to proceed with the LS formalism, we utilize the identity operator in the two-excitation subspace

$$\hat{I}_2 = \hat{I}_2^x \otimes |\mathbf{0}\rangle\langle\mathbf{0}| + \hat{I}_1^x \otimes \sum_{i=0}^{N-1}|d_i\rangle\langle d_i| + \hat{I}_0^x \otimes \sum_{j\le k}|d_jd_k\rangle\langle d_jd_k|\,, \tag{4.37}$$

where

$$\hat{I}_n^x = \int dx_1...dx_n\,|x_1...x_n\rangle\langle x_1...x_n|\,, n>0 \tag{4.38}$$

and $\hat{I}_0^x = |0\rangle\langle 0|$ is the projection to the zero-photon state in the waveguide. Furthermore, we define

$$|d_i\rangle = \hat{d}_i^\dagger\,|\mathbf{0}\rangle\,, \tag{4.39}$$

$$|d_id_j\rangle = \hat{d}_i^\dagger\hat{d}_j^\dagger\,|\mathbf{0}\rangle\,, \tag{4.40}$$

$$|d_id_i\rangle = \frac{1}{\sqrt{2}}\left(\hat{d}_i^\dagger\right)^2|\mathbf{0}\rangle\,. \tag{4.41}$$

By inserting the identity operator $\hat{I}_2$ into Eq. (4.35), we obtain

$$\begin{aligned}
|\psi_2(k_1,k_2);\alpha_1,\alpha_2\rangle &= |\phi_2(k_1,k_2);\alpha_1,\alpha_2\rangle + \hat{G}(E)\sum_{i=0}^{N-1}\hat{\mathcal{V}}_i\hat{I}_2\,|\psi_2(k_1,k_2);\alpha_1,\alpha_2\rangle \\
&= |\phi_2(k_1,k_2);\alpha_1,\alpha_2\rangle + \frac{U}{2}\hat{G}(E)\sum_{i=0}^{N-1}\hat{d}_i^\dagger\hat{d}_i(\hat{d}_i^\dagger\hat{d}_i-1)\times \\
&\quad \hat{I}_0^x\otimes\sum_{j\le k}|d_jd_k\rangle\,\langle d_jd_k|\psi_2(k_1,k_2);\alpha_1,\alpha_2\rangle \\
&= |\phi_2(k_1,k_2);\alpha_1,\alpha_2\rangle + U\hat{G}(E)\times \\
&\quad \hat{I}_0^x\otimes\sum_{i=0}^{N-1}|d_id_i\rangle\,\langle d_id_i|\psi_2(k_1,k_2);\alpha_1,\alpha_2\rangle \\
&= |\phi_2(k_1,k_2);\alpha_1,\alpha_2\rangle + U\hat{G}(E)\times \\
&\quad \sum_{i=0}^{N-1}|0;d_id_i\rangle\,\langle 0;d_id_i|\psi_2(k_1,k_2);\alpha_1,\alpha_2\rangle\,, \qquad (4.42)
\end{aligned}$$

where we have defined $|0;d_id_i\rangle = |0\rangle\otimes|d_id_i\rangle$. We have used the bosonic commutation relations of $\hat{d}_j$ and $\hat{d}_j^\dagger$ in the above derivation.

To proceed further, we operate with $\langle 0;d_id_i|$ on the left of Eq. (4.42), yielding

$$\begin{aligned}
&\langle 0;d_id_i|\psi_2(k_1,k_2);\alpha_1,\alpha_2\rangle = \\
&\langle 0;d_id_i|\phi_2(k_1,k_2);\alpha_1,\alpha_2\rangle + U\sum_{j=0}^{N-1}G_{ij}\,\langle 0;d_jd_j|\psi_2(k_1,k_2);\alpha_1,\alpha_2\rangle\,, \qquad (4.43)
\end{aligned}$$

where we have set $G_{ij} = \langle 0;d_id_i|\,\hat{G}(E)\,|0;d_jd_j\rangle$. We write Eq. (4.43) in matrix form, and then invert the equation. This provides us with the following result:

$$\begin{pmatrix}\langle 0;d_1d_1|\psi_2(k_1,k_2);\alpha_1,\alpha_2\rangle\\ \langle 0;d_2d_2|\psi_2(k_1,k_2);\alpha_1,\alpha_2\rangle\\ \langle 0;d_3d_3|\psi_2(k_1,k_2);\alpha_1,\alpha_2\rangle\end{pmatrix} = (I-UG)^{-1}\begin{pmatrix}\langle 0;d_1d_1|\phi_2(k_1,k_2);\alpha_1,\alpha_2\rangle\\ \langle 0;d_2d_2|\phi_2(k_1,k_2);\alpha_1,\alpha_2\rangle\\ \langle 0;d_3d_3|\phi_2(k_1,k_2);\alpha_1,\alpha_2\rangle\end{pmatrix}, \quad (4.44)$$

where G is a 3×3 matrix with elements G_{ij}. With this definition, Eq. (4.42)

is written as

$$\begin{aligned}|\psi_2(k_1,k_2);\alpha_1,\alpha_2\rangle =& |\phi_2(k_1,k_2);\alpha_1,\alpha_2\rangle + U\hat{G}(E)\times \\ & \sum_{i=0}^{N-1} |0;d_id_i\rangle \langle 0;d_id_i|\psi_2(k_1,k_2);\alpha_1,\alpha_2\rangle \\ =& |\phi_2(k_1,k_2);\alpha_1,\alpha_2\rangle + U\sum_{i=0}^{N-1}\sum_{j=0}^{N-1} \hat{G}(E)\,|0;d_id_i\rangle \times \\ & \left[(I-UG)^{-1}\right]_{ij} \langle 0;d_jd_j|\phi_2(k_1,k_2);\alpha_1,\alpha_2\rangle\,, \end{aligned} \tag{4.45}$$

Taking the limit $U \to \infty$ provides us the formula for the two-photon eigenstate with the nonlinear correction

$$\begin{aligned}|\psi_2(k_1,k_2);\alpha_1,\alpha_2\rangle =& |\phi_2(k_1,k_2);\alpha_1,\alpha_2\rangle - \sum_{i=0}^{N-1}\sum_{j=0}^{N-1} \hat{G}(E)\,|0;d_id_i\rangle \times \\ & \left(G^{-1}\right)_{ij} \langle 0;d_jd_j|\phi_2(k_1,k_2);\alpha_1,\alpha_2\rangle\,. \end{aligned} \tag{4.46}$$

Let us calculate the terms in Eq. (4.46). The final term in this formula is evaluated by operating with $\langle 0;d_jd_j|$ on the two-photon noninteracting eigenstate of Eq. (4.32). Using Eqs. (4.32) and (4.34), we obtain

$$\begin{aligned}\langle 0;d_jd_j|\phi_2(k_1,k_2);\alpha_1,\alpha_2\rangle &= \sum_{k=0}^{N-1} e_k^{\alpha_1}(k_1)e_k^{\alpha_2}(k_2)\,\langle d_jd_j|d_kd_k\rangle \\ &= e_j^{\alpha_1}(k_1)e_j^{\alpha_2}(k_2). \end{aligned} \tag{4.47}$$

For the calculation of the remaining elements of Eq. (4.46), we present the two-photon identity operator in momentum space

$$\hat{I}_2' = \sum_{\alpha,\alpha'=\mathrm{R,L}} \int dk_1 \int dk_2\, |\phi_2(k_1,k_2);\alpha,\alpha'\rangle \langle \phi_2(k_1,k_2);\alpha,\alpha'|\,. \tag{4.48}$$

The term $\hat{G}(E)\,|0;d_id_i\rangle$ and the elements G_{ij} of the G matrix from Eq. (4.46)

and can be evaluated with help of the identity operator $\hat{I}_2'$ as

$$\begin{aligned}
\hat{G}(E)\left|0;d_id_i\right\rangle =&\hat{G}(E)\hat{I}_2'\left|0;d_id_i\right\rangle \\
=&\sum_{\alpha,\alpha'=\mathrm{R,L}}\int dk_1\int dk_2\frac{1}{E-\hbar vk_1-\hbar vk_2+i\epsilon}\times \\
&\left|\phi_2(k_1,k_2);\alpha,\alpha'\right\rangle\left\langle\phi_2(k_1,k_2);\alpha,\alpha'|0;d_id_i\right\rangle \\
=&\sum_{\alpha,\alpha'=\mathrm{R,L}}\int dk_1\int dk_2\frac{1}{E-\hbar vk_1-\hbar vk_2+i\epsilon}\times \\
&\left|\phi_2(k_1,k_2);\alpha,\alpha'\right\rangle\left[e_i^{\alpha}(k_1)e_i^{\alpha'}(k_2)\right]^*, \qquad (4.49)\\
G_{ij}=&\left\langle 0;d_id_i\right|\hat{G}(E)I_2'\left|0;d_jd_j\right\rangle \\
=&\sum_{\alpha,\alpha'=\mathrm{R,L}}\int dk_1\int dk_2\frac{1}{E-\hbar vk_1-\hbar vk_2+i\epsilon}\times \\
&\left\langle 0;d_id_i|\phi_2(k_1,k_2);\alpha,\alpha'\right\rangle\left\langle\phi_2(k_1,k_2);\alpha,\alpha'|0;d_jd_j\right\rangle \\
=&\sum_{\alpha,\alpha'=\mathrm{R,L}}\int dk_1\int dk_2\frac{1}{E-\hbar vk_1-\hbar vk_2+i\epsilon}\times \\
&e_i^{\alpha}(k_1)e_i^{\alpha'}(k_2)\left[e_j^{\alpha}(k_1)e_j^{\alpha'}(k_2)\right]^*, \qquad (4.50)
\end{aligned}$$

where '$*$' denotes the complex conjugate. We have used the result of Eq. (4.47) in the simplification of the integrands.

4.2.1 Two-photon eigenstate in the position basis

The two-photon states exhibit various interesting correlation properties in their position variables. Here we introduce the wavefunction for the two-photon scattering eigenstate with the nonlinear correction. The following single-photon result is useful in the forthcoming calculations:

$$\begin{aligned}
\left\langle x_1;\mathbf{0}|\phi_1(k_1);\alpha\right\rangle =&\sum_{\alpha'=\mathrm{R,L}}\left\langle x_1\right|\int dx\,\phi_{\alpha'}^{\alpha}(k_1,x)\hat{a}_{\alpha'}^{\dagger}(x)\left|0\right\rangle \\
=&\sum_{\alpha'=\mathrm{R,L}}\int dx\,\phi_{\alpha'}^{\alpha}(k_1,x)\left\langle x_1\right|\hat{a}_{\alpha'}^{\dagger}(x)\left|0\right\rangle \\
=&\sum_{\alpha'=\mathrm{R,L}}\int dx\,\phi_{\alpha'}^{\alpha}(k_1,x)\delta(x-x_1) \\
=&\phi_{\mathrm{R}}^{\alpha}(k_1,x_1)+\phi_{\mathrm{L}}^{\alpha}(k_1,x_1), \qquad (4.51)
\end{aligned}$$

where $|x_1\rangle$ is a state with a single photon at location x_1. With this result, the symmetrized two-photon noninteracting state of Eq. (4.32) in the position basis becomes

$$\begin{aligned}\langle x_1 x_2; \mathbf{0}|\phi_2(k_1,k_2);\alpha_1,\alpha_2\rangle \\ &= \frac{1}{2}\left\{\left[\phi_{\mathrm{R}}^{\alpha_1}(k_1,x_1)+\phi_{\mathrm{L}}^{\alpha_1}(k_1,x_1)\right]\left[\phi_{\mathrm{R}}^{\alpha_2}(k_2,x_2)+\phi_{\mathrm{L}}^{\alpha_2}(k_2,x_2)\right]\right. \\ &\quad \left.+\,(x_1\leftrightarrow x_2)\right\}. \end{aligned} \tag{4.52}$$

The two-photon state [see Eq. (4.46)] in the coordinate basis thus reads

$$\begin{aligned}\langle x_1 x_2; \mathbf{0}|\psi_2(k_1,k_2);\alpha_1,\alpha_2\rangle &= \langle x_1 x_2; \mathbf{0}|\phi_2(k_1,k_2);\alpha_1,\alpha_2\rangle \\ &\quad -\sum_{i=0}^{N-1}\sum_{j=0}^{N-1}\langle x_1 x_2;\mathbf{0}|\,\hat{G}(E)\,|0;d_i d_i\rangle\left(G^{-1}\right)_{ij}\times \\ &\quad \langle 0;d_j d_j|\phi_2(k_1,k_2);\alpha_1,\alpha_2\rangle \\ &= \langle x_1 x_2; \mathbf{0}|\phi_2(k_1,k_2);\alpha_1,\alpha_2\rangle \\ &\quad -\sum_{i=0}^{N-1}\sum_{j=0}^{N-1}G_i(x_1,x_2)\left(G^{-1}\right)_{ij}\langle 0;d_j d_j|\phi_2(k_1,k_2);\alpha_1,\alpha_2\rangle, \end{aligned} \tag{4.53}$$

where we have defined

$$\begin{aligned}G_i(x_1,x_2) &= \langle x_1 x_2;\mathbf{0}|\,\hat{G}(E)\hat{I}_2'\,|0;d_j d_j\rangle \\ &= \sum_{\alpha,\alpha'=\mathrm{R,L}}\int dk_1\int dk_2\frac{1}{E-\hbar v k_1-\hbar v k_2+i\epsilon}\times \\ &\quad \langle x_1 x_2;\mathbf{0}|\phi_2(k_1,k_2);\alpha,\alpha'\rangle\langle\phi_2(k_1,k_2);\alpha,\alpha'|0;d_i d_i\rangle. \end{aligned} \tag{4.54}$$

The information about the state of the qubits is lost in the calculation of the two-photon wavefunction of Eq. (4.53). However, the two-photon wavefunction is of interest in experiments in which only the properties of the photons, such as their phases, are of interest.

4.2.2 Markovian approximation

Solving the full two-photon state requires inserting the wavefunctions from Eqs. (4.13)–(4.16), and the amplitudes from the solutions of Eqs. (4.17)–(4.25) into the Green's functions (4.49) and (4.50). After performing these steps, one ends up with integrals with no known analytic solution.

However, these integrals may be simplified and analytically solved with help of the Markovian approximation. In this approximation, we assume

that the interaction between the qubits and the photons is instantaneous, and that the propagation time of emitted photons between the qubits can be neglected. This is true, if the qubits are placed close to each other.

Comparison between the Markovian and the non-Markovian solutions on the qubit dynamics was conducted in Ref. [29]. They concluded that the Markovian approximation is valid if the separation of the qubits does not exceed approximately $5\lambda/2$, where λ is the wavelength of the photon. In practice, the approximation is carried out by replacing the wavenumber k appearing in the complex exponentials in Eqs. (4.49) and (4.50) with $k_0 = 2\pi/\lambda$, where λ is the wavelength of the photons. [23, 29]

Within this approximation, the integrals under evaluation contain only polynomials in both the numerator and the denominator, with the degree of the denominator being greater than the degree of the numerator. The integral over the real axis can be transformed into a path integral over the upper complex half space, since the path integral of the semicircle is known to vanish for integrals of this type at the limit where the radius of the semicircle is taken into infinity [35]. The integrals can be then evaluated using the residue theorem

$$\oint_C dz\, f(z) = 2\pi i \sum_{k=0}^{N} \mathrm{Res}(f, z_k), \tag{4.55}$$

where z is a complex variable, C is the integration path over the upper complex plane, z_k are the poles encircled by C, and $f : \mathbb{C}\backslash\{z_0, ..., z_N\} \to \mathbb{C}$ is a function which is complex differentiable in its domain. The formula for the kth degree residue of f at z_k is given by [35]

$$\mathrm{Res}(f, z_k) = \frac{1}{(k-1)!} \lim_{z \to z_k} \frac{d^{k-1}}{dz^{k-1}} \left[(z - z_k)^k f(z) \right]. \tag{4.56}$$

4.2.3 Summary of the Green's function method

In this section, we present step-by-step instructions how to calculate the two-photon wavefunction with the nonlinear correction.

1. Construct the single-photon scattering eigenstate for the system, and calculate the scattering coefficients with the Schrödinger equation (see Secs. 4.1.1 and 4.1.2 and Appendix A).

2. Replace the wavenumber k in the complex exponentials appearing in the previously calculated scattering coefficients with $k_0 = 2\pi/\lambda$, where λ is the wavelength of the photons.

3. Using the coefficients from the previous step, construct the matrix G with elements G_{ij} as defined in Eq. (4.50). The integrals are calculated with the residue theorem (see Sec. 4.2.2).

4. Construct the two-photon noninteracting wavefunction with Eq. (4.52) by using the single-photon wavefunctions and coefficients obtained in Steps 1 and 2.

5. Construct the functions $G_i(x_1, x_2)$ with help of the Eq. (4.54). The integrals are calculated with the residue theorem similarly as in Step 3.

6. Using the results acquired in Steps 3, 4, and 5, calculate the two-photon wavefunction with Eq. (4.53).

Chapter 5

Results

In this chapter, by utilizing methods outlined in Ch. 4, we calculate the scattering properties of one- and two-photon input states in a one-dimensional superconducting transmission line, to which three superconducting qubits are capacitively coupled. Finally, based on these results, we discuss the implementation of conditional-phase-shift and controlled-Z gates for a microwave photonic quantum computer.

5.1 Nonlinear phase shifter

We consider a system with three superconducting qubits with transition frequency Ω capacitively coupled to an infinite transmission line. The circuit diagram of the system is presented in Fig. 5.1. The system is one dimensional and symmetric with respect to the middle qubit, and the separation of qubits is set to $\lambda/4$, where λ is the wavelength of the incident photons. The decay rate to the waveguide continuum (see Appendix A for definition) is Γ for the leftmost and rightmost qubits, and $\gamma\Gamma$ for the middle qubit. Here, γ is a dimensionless constant hereby referred to as the coupling ratio.

We calculate the single-photon scattering amplitudes from Eqs. (4.17)–(4.25) by setting $L = \lambda/4$. The amplitudes become

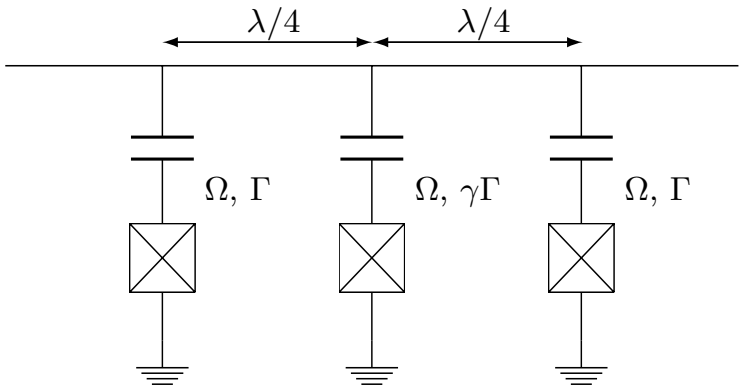

Figure 5.1: Circuit diagram of the nonlinear phase shifter. Three superconducting qubits are capacitively coupled to an infinite transmission line. The qubits are separated by length $\lambda/4$, Ω is the transition frequency of the qubits, Γ is the decay rate to the transmission line, and γ is the coupling ratio.

$$t_3^{\mathrm{R}}(k) = t_3^{\mathrm{L}}(k) = \frac{2\delta^3}{(i\Gamma+\delta)\left[2\delta^2-\gamma\Gamma(\Gamma-i\delta)\right]}, \tag{5.1}$$

$$t_{12}^{\mathrm{R}}(k) = t_{23}^{\mathrm{L}}(k) = \frac{i\delta\left[\delta(i\Gamma+2\delta)-\gamma\Gamma(\Gamma-i\delta)\right]}{(\Gamma-i\delta)\left[\gamma\Gamma(\Gamma-i\delta)-2\delta^2\right]}, \tag{5.2}$$

$$t_{23}^{\mathrm{R}}(k) = t_{12}^{\mathrm{L}}(k) = -\frac{(\Gamma-2i\delta)\delta^2}{(\Gamma-i\delta)\left[\gamma\Gamma(\Gamma-i\delta)-2\delta^2\right]}, \tag{5.3}$$

$$r_3^{\mathrm{R}}(k) = r_3^{\mathrm{L}}(k) = \frac{\Gamma\left[\gamma(\Gamma^2+\delta^2)-2\delta^2\right]}{(\Gamma-i\delta)\left[\gamma\Gamma(\Gamma-i\delta)-2\delta^2\right]}, \tag{5.4}$$

$$r_{12}^{\mathrm{R}}(k) = r_{23}^{\mathrm{L}}(k) = \frac{\Gamma\delta\left[i\gamma\Gamma+(\gamma-1)\delta\right]}{(\Gamma-i\delta)\left[\gamma\Gamma(\Gamma-i\delta)-2\delta^2\right]}, \tag{5.5}$$

$$r_{23}^{\mathrm{R}}(k) = r_{12}^{\mathrm{L}}(k) = -\frac{\Gamma\delta^2}{(\Gamma-i\delta)\left[\gamma\Gamma(\Gamma-i\delta)-2\delta^2\right]}, \tag{5.6}$$

$$e_1^{\mathrm{R}}(k) = e_3^{\mathrm{L}}(k) = \frac{\sqrt{v\Gamma}\left[\delta^2-\gamma\Gamma(\Gamma-i\delta)\right]}{\sqrt{\pi}(\Gamma-i\delta)\left[\gamma\Gamma(\Gamma-i\delta)-2\delta^2\right]}, \tag{5.7}$$

$$e_2^{\mathrm{R}}(k) = e_2^{\mathrm{L}}(k) = \frac{\sqrt{v\Gamma}\delta}{\sqrt{\pi}\left[2\delta^2-\gamma\Gamma(\Gamma-i\delta)\right]}, \tag{5.8}$$

$$e_3^{\mathrm{R}}(k) = e_1^{\mathrm{L}}(k) = -\frac{\sqrt{v\Gamma}\delta^2}{\sqrt{\pi}(\Gamma-i\delta)\left[\gamma\Gamma(\Gamma-i\delta)-2\delta^2)\right]}, \tag{5.9}$$

where $\delta = vk - \Omega$ is the detuning between the frequency of the photons and the transition frequency of the qubits.

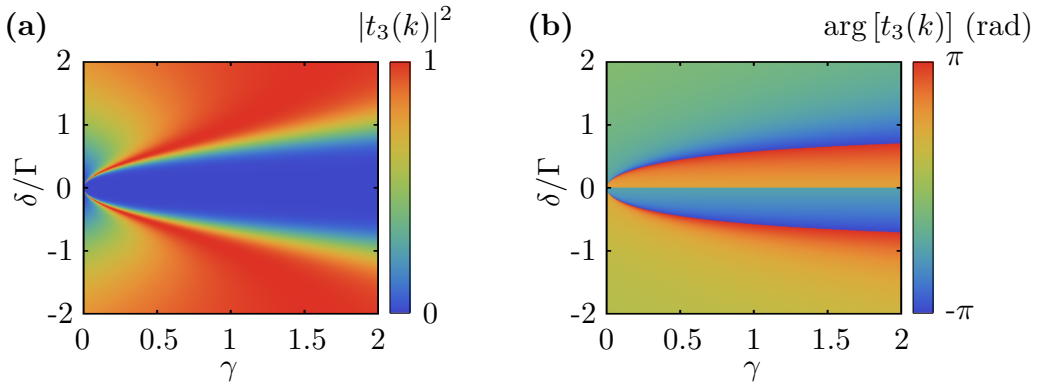

Figure 5.2: (a) Absolute value squared and (b) phase of the single-photon transmission coefficient $t_3(k)$ as a function of coupling ratio γ and detuning $\delta = vk - \Omega$. The detuning is given in the units of the decay rate Γ. The distance between the qubits is set to $L = \lambda/4$.

5.1.1 Single-photon transmission

We assume a single photon with wavenumber k propagating initially from the left. As it passes the three-qubit system, it acquires a phase $\theta_1(k) \equiv \arg[t_3(k)]$. Here, the transmission coefficient $t_3(k)$ is defined with help of the definitions from Eq. (4.17) as $t_3(k) \equiv t_3^{\mathrm{R}}(k) = t_3^{\mathrm{L}}(k)$. The absolute value squared and the phase of the transmission coefficient $t_3(k)$ are presented in Fig. 5.2. We note that there exists a wide range of parameters for unity or near-unity transmission. With larger detuning δ, there is less interaction between the photon and the qubits, and hence the transmission probability typically increases as the absolute value of the detuning δ increases.

In the following, we are interested in the region where zero reflection occurs, since the backscattering from the components on a quantum circuit could possibly lead to non-desirable interferences and errors. We require that the absolute value squared of Eq. (5.1) equals to unity, i.e., that there is a full single-photon transmission. This requirement provides a relation for the detuning between the photons and qubits frequencies

$$\delta_{\mathrm{f}}(\gamma, \Gamma) = \pm\sqrt{\frac{\gamma}{2-\gamma}}\Gamma, \tag{5.10}$$

assuring that the reflectance is zero. This can be verified by calculating the reflection coefficient $r_3(k) \equiv r_3^{\mathrm{R}}(k) = r_3^{\mathrm{L}}(k)$ of Eq. (5.4) with the detuning set to $\delta_{\mathrm{f}}(\gamma, \Gamma)$, yielding zero for all values of γ and Γ. Furthermore, by requiring that the detuning of Eq. (5.10) is real-valued and finite, the coupling ratio is restricted to $0 \leq \gamma < 2$.

The phase shift of the single-photon input state with the detuning of Eq. (5.10), corresponding to the wavenumber $k_\mathrm{f} \equiv [\delta_\mathrm{f}(\gamma,\Gamma)+\Omega]/v$, is given by

$$\theta_1(k_\mathrm{f}) = \arg\left[t_3(k_\mathrm{f})\right] = \pm\arctan\left(\frac{\sqrt{2\gamma-\gamma^2}}{1-\gamma}\right). \tag{5.11}$$

5.1.2 Two-photon transmission

The wavefunctions of the transmitted and reflected two-photon states are calculated from Eq. (4.53). We assume that the incident photons are right-going plane waves with equal energies $E = \hbar v k$. The incident two-photon wavefunction in the region $x_1, x_2 < -L$ is given by

$$\begin{aligned}\phi_2^\mathrm{in}(k,x_1,x_2) &= \frac{1}{2\left(\sqrt{2\pi}\right)^2}\left[e^{i(kx_1+kx_2)} + (x_1 \leftrightarrow x_2)\right] \\ &= \frac{1}{2\pi}e^{i(kx_1+kx_2)}.\end{aligned} \tag{5.12}$$

The noninteracting term in the transmitted wavefunction is calculated with Eq. (4.52) by setting $\alpha_1 = \alpha_2 = \mathrm{R}$, and taking into account only right-going waves in the region $x_1, x_2 > L$. Hence, the noninteracting transmitted wavefunction is written as

$$\begin{aligned}\phi_2^\mathrm{T}(k,x_1,x_2) &= \frac{1}{2}\left[\phi_\mathrm{R}^\mathrm{R}(k,x_1)\phi_\mathrm{R}^\mathrm{R}(k,x_2) + (x_1 \leftrightarrow x_2)\right] \\ &= t_3(k)t_3(k)\phi_2^\mathrm{in}(k,x_1,x_2),\end{aligned} \tag{5.13}$$

where the single-photon transmission coefficient $t_3(k)$ is given by Eq. (5.1). We calculate the two-photon wavefunction including the nonlinear correction with the help of the Eq. (4.53). The transmitted wavefunction in the region $x_1, x_2 > L$ becomes

$$\psi_2^\mathrm{T}(k,x_1,x_2) = \left[t_3(k)t_3(k) + B^\mathrm{T}(k,x_2-x_1)\right]\phi_2^\mathrm{in}(k,x_1,x_2), \tag{5.14}$$

where $B^\mathrm{T}(k,x_2-x_1)$ is the nonlinear correction in the transmitted wavefunction. The analytical solution for the nonlinear correction with $x_1 = x_2$ is given in Appendix B. We note that in general this term depends on position variables of photons, or rather their difference, $|x_2 - x_1|$.

Let us assume that the position difference is zero, i.e., $x_1 = x_2$. The complex phases of the two-photon transmission coefficient with and without the nonlinear correction, as well as their difference are presented in Fig. 5.3(a), with the wavenumbers of the photons set to $k = k_\mathrm{f}$ corresponding to the

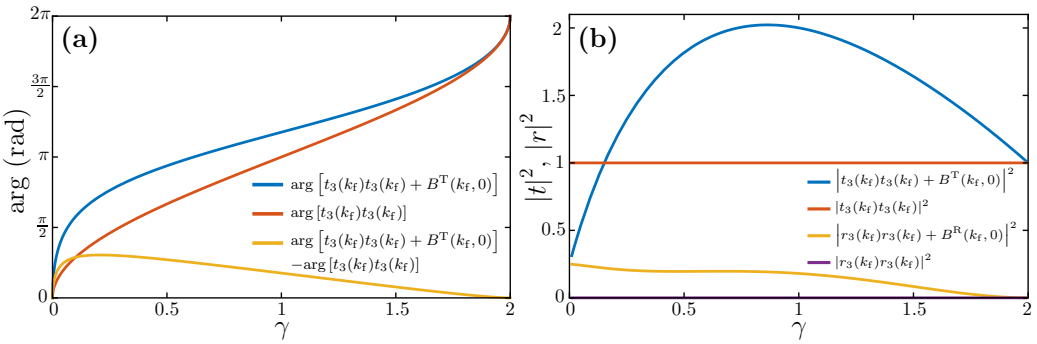

Figure 5.3: Nonlinear effects in the two-photon wavefunction, with the position difference set to zero, i.e., $x_1 = x_2$, and the wavenumbers set to correspond to the full single-photon transmission, $k = k_\mathrm{f}$. (a) Complex phases of the transmission coefficients with and without the nonlinear term, and their difference as a function of the coupling ratio γ. (b) The absolute value squared of the transmission and reflection coefficients with and without the corresponding nonlinear term as a function of the coupling ratio γ.

full single-photon transmission. We limit the values of the coupling ratio to $0 \leq \gamma < 2$, since full single-photon transmission can only be achieved with these values, as was discussed in Sec. 5.1.1. We find the maximum nonlinear phase shift to be approximately $3\pi/10$ radians, achieved with the coupling ratio $\gamma_\mathrm{max} \approx 0.21$. The nonlinearity vanishes as γ approaches the value 2.

5.1.3 Two-photon reflection

Assuming the input state defined in Eq. (5.12), the reflected wavefunction in the region $x_1, x_2 < -L$ is calculated using Eq. (4.53), yielding

$$\psi_2^\mathrm{R}(k, x_1, x_2) = \left[r_3(k)r_3(k) + B^\mathrm{R}(k, x_2 - x_1)\right] \phi_2^\mathrm{out}(-k, x_1, x_2), \qquad (5.15)$$

where the reflection coefficient $r_3(k)$ is defined by Eq. (5.4), and $B^\mathrm{R}(k, x_2 - x_1)$ is the nonlinear correction for the reflected two-photon wavefunction. The analytical formula for B^R for $x_1 = x_2$ is given in Appendix B. The negative sign appearing in the argument of ϕ_2^out is introduced since the reflected plane wave travels in a direction opposite to the incident wave.

Setting $k = k_\mathrm{f}$ and $x_1 = x_2$, we present the absolute value squared of the transmission and reflection coefficients of the two-photon states with and without the nonlinear terms in Fig. 5.3(b). In the noninteracting case, the reflection naturally vanishes, since there is no single-photon reflection if $k = k_\mathrm{f}$. However, if the nonlinear correction is taken into account, some

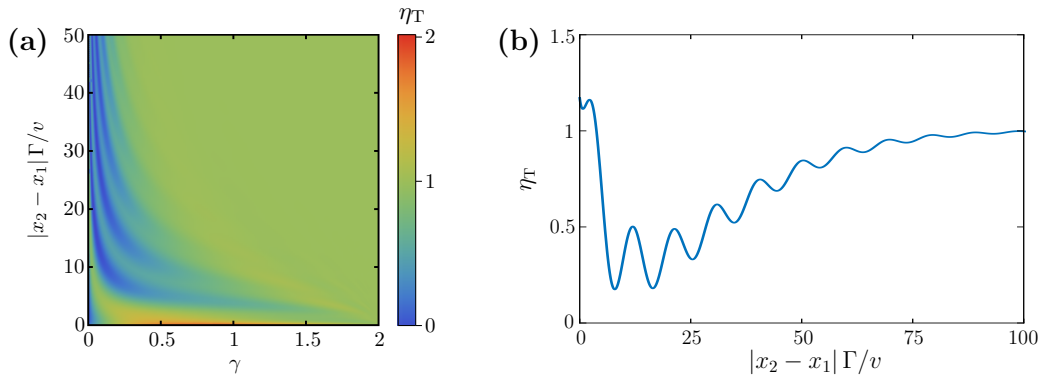

Figure 5.4: (a) Ratio of the transmitted probability densities with and without the nonlinear correction, η_T, as a function of coupling ratio γ and the difference in the two-photon position coordinates, $|x_2 - x_1|$. (b) The ratio η_T traced along $\gamma = \gamma_{max}$. The wavenumber is set so that full single-photon transmission occurs, i.e., $k = k_f$.

amount of reflected amplitude remains. The reflection is strongest with the smallest values of the coupling ratio γ, and decreases to zero as $\gamma \to 2$. However, in this limit also the nonlinear phase shift vanishes.

5.1.4 Spatial correlations

In general, the nonlinear correction terms B^T and B^R in the two-photon wavefunctions depend on the separation of photons, $|x_2 - x_1|$. Hence the two-photon wavefunction itself also depends on the separation. In this section, we characterize the spatial correlations arising in the two-photon state.

Transmission

The correlations in the transmitted two-photon states can be characterized by the ratio of the probability densities of the transmitted wavefunctions with and without the nonlinear correction as [36]

$$\begin{aligned}\eta_T(k, x_1, x_2) &= \frac{\left|\psi_2^T(k, x_1, x_2)\right|^2}{\left|t_3(k)t_3(k)\phi_2^{in}(k, x_1, x_2)\right|^2} \\ &= \frac{\left|t_3(k)t_3(k) + B^T(k, x_2 - x_1)\right|^2}{\left|t_3(k)t_3(k)\right|^2},\end{aligned} \tag{5.16}$$

where the numerator and the denominator correspond to nonlinear and linear two-photon transmission probability densities, respectively.

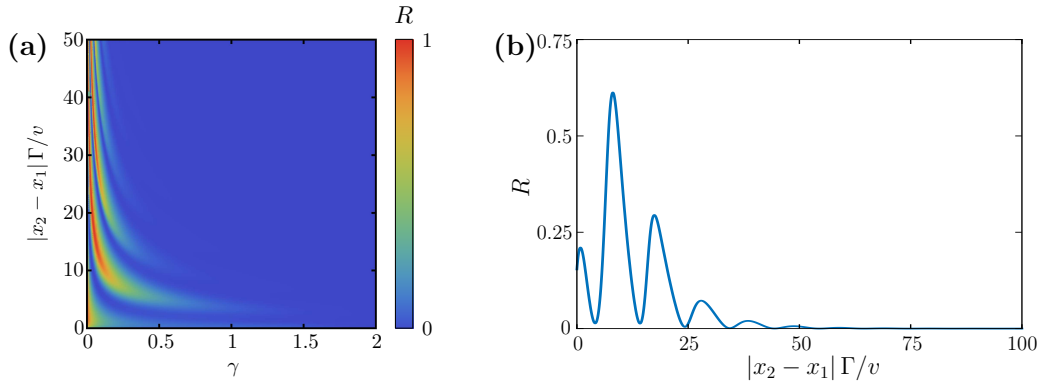

Figure 5.5: (a) Ratio of the reflected probability density and the total probability density, R, as a function of the coupling ratio γ and the difference in the two-photon position coordinates, $|x_2 - x_1|$. (b) The ratio R traced along $\gamma = \gamma_{\max}$. The wavenumber is set such that full single-photon transmission occurs, i.e., $k = k_{\mathrm{f}}$.

In the following we assume the wavenumbers of the photons to correspond to the full single-photon transmission, i.e., $k = k_{\mathrm{f}}$. The ratio η_{T} is shown in Fig. 5.4 as a function of the coupling ratio γ and the position difference $|x_2 - x_1|$. We also present the ratio η_{T} traced along $\gamma = \gamma_{\max}$, since we found that the nonlinear phase shift for colocated photons was most significant near this value.

We note that oscillations appear in η_{T} as it is traced along $\gamma = \gamma_{\max}$. For small separations we have $\eta_{\mathrm{T}} > 1$, corresponding to photon bunching [36]. With increasing the difference $|x_2 - x_1|$, the ratio starts to oscillate and assumes values less than unity.

For large $|x_2 - x_1|$, η_{T} saturates to unity. This is physically intuitive since photons with a large separation hardly ever simultaneously reside at the locations of the qubits, and hence interact weakly with each other.

Reflection

The amount of reflection in the two-photon case can be calculated by evaluating the ratio of the probability amplitudes as

$$\begin{aligned} R(k, x_1, x_2) &= \frac{\left|\psi_2^{\mathrm{R}}(k, x_1, x_2)\right|^2}{\left|\psi_2^{\mathrm{R}}(k, x_1, x_2)\right|^2 + \left|\psi_2^{\mathrm{T}}(k, x_1, x_2)\right|^2} \\ &= \frac{\left|r_3(k) r_3(k) + B^{\mathrm{R}}(k, x_2 - x_1)\right|^2}{\left|r_3(k) r_3(k) + B^{\mathrm{R}}(k, x_2 - x_1)\right|^2 + \left|t_3(k) t_3(k) + B^{\mathrm{T}}(k, x_2 - x_1)\right|^2}. \end{aligned} \tag{5.17}$$

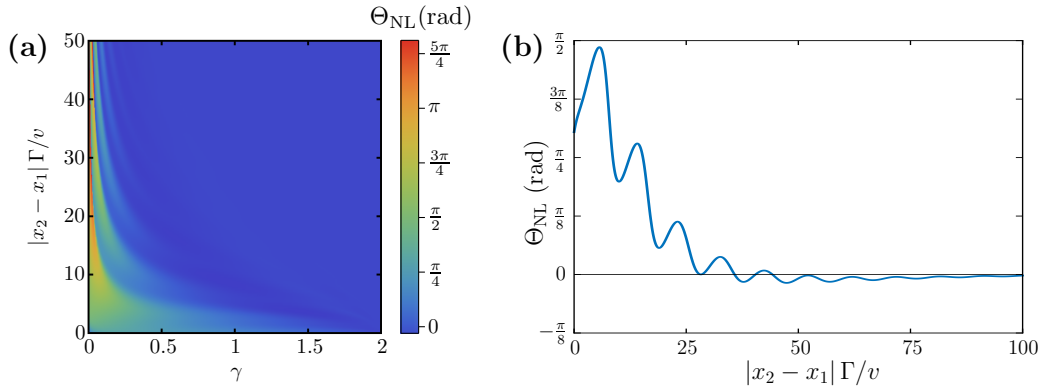

Figure 5.6: Amount of nonlinearity in the phase of the two-photon wavefunction, Θ_{NL}, (a) represented as a function of the coupling ratio γ and the difference in two-photon position coordinates $|x_2 - x_1|$, and (b) traced along $\gamma = \gamma_{\mathrm{max}}$.

We set the wavenumbers of the photons again to $k = k_{\mathrm{f}}$, corresponding to full single-photon transmission. The amount of reflection is shown as a function of the coupling ratio γ and the difference $|x_2 - x_1|$ in Fig. 5.5(a), and traced along $\gamma = \gamma_{\mathrm{max}}$ in Fig. 5.5(b). The observed behavior seems qualitatively similar to the one corresponding to the ratio η_{T}. Full reflection can only occur for small values of the coupling ratio γ. The linear regime for R corresponds to zero reflection. For $\gamma = \gamma_{\mathrm{max}}$, reflection is essentially zero after $|x_2 - x_1| > 50v/\Gamma$.

Nonlinearity in phase

The nonlinearity in the phase of the two-photon state also depends on the spatial separation of photons. We quantify this nonlinearity for photons with separation $|x_2 - x_1| \neq 0$ by calculating the difference in the phase between the full two-photon wavefunction and the noninteracting two-photon wavefunction as

$$\Theta_{\mathrm{NL}}(k, x_1, x_2) = \arg\left[\psi_2^{\mathrm{T}}(k, x_1, x_2)\right] - \arg\left[\phi_2^{\mathrm{T}}(k, x_1, x_2)\right], \tag{5.18}$$

where ψ_2^{T} and ϕ_2^{T} are the two-photon wavefunctions with and without the nonlinear correction, defined by Eqs. (5.14) and (5.13), respectively.

We set the wavenumbers of the photons to correspond to the full single-photon transmission, $k = k_{\mathrm{f}}$. The nonlinearity in phase is shown in Fig. 5.6(a) as a function the coupling ratio γ and the separation $|x_2 - x_1|$. Qualitatively, the observed behavior resembles that for the ratios η_{T} and R with

oscillations and a similar linear regime. In the linear regime, the nonlinearity in phase is zero. The nonlinearity in the phase traced along $\gamma = \gamma_{\max}$ is shown in Fig. 5.6(b). It is most prominent with short distances between photons, maximum value being close to $\pi/2$ radians. Nonlinearity becomes essentially zero for $|x_2 - x_1| > 100v/\Gamma$.

5.1.5 Response of the device

In this section, we show how one- and two-photon input states transform in the nonlinear phase shifter device. For the single-photon case, we take the input state

$$|1\rangle_{\text{in}} = \int dx\, \phi_1^{\text{in}}(k,x)\hat{a}_{\text{R}}^\dagger(x)\,|0\rangle\,, \tag{5.19}$$

where the input wavefunction is the plane-wave state $\phi_1^{\text{in}}(k,x) = e^{ikx}/\sqrt{2\pi}$. After interacting with the nonlinear phase shifter, the transmitted state becomes

$$|1\rangle_{\text{out}} = \int dx\, \phi_1^{\text{in}}(k,x)t_3(k)\hat{a}_{\text{R}}^\dagger(x)\,|0\rangle = t_3(k)\,|1\rangle_{\text{in}}\,. \tag{5.20}$$

Thus, the single-photon phase shift for a photon with wavenumber k is given by $\theta_1(k) = \arg[t_3(k)]$, where the transmission coefficient is defined by Eq. (4.17). For full single-photon transmission with $k = k_{\text{f}}$, an analytical solution for the phase shift is given in Eq. (5.11).

The two-photon input state for photons with equal wavenumbers k is taken to be

$$|2\rangle_{\text{in}} = \int dx_1 \int dx_2\, \phi_2^{\text{in}}(k,x_1,x_2)\hat{a}_{\text{R}}^\dagger(x_1)\hat{a}_{\text{R}}^\dagger(x_2)\,|0\rangle\,, \tag{5.21}$$

where $\phi_2^{\text{in}}(k,x_1,x_2)$ is the two-photon input wavefunction defined by Eq. (5.12). The two-photon state transforms to

$$\begin{aligned}|2\rangle_{\text{out}} = \int dx_1 \int dx_2\, \phi_2^{\text{in}}(k,x_1,x_2)\,&[t_3(k)t_3(k)\\ &+B^{\text{T}}(k,x_2-x_1)]\,\hat{a}_{\text{R}}^\dagger(x_1)\hat{a}_{\text{R}}^\dagger(x_2)\,|0\rangle\,.\end{aligned} \tag{5.22}$$

This form is problematic since the nonlinear correction depends on the spatial separation of photons, and hence it cannot be taken out of the integral. Assuming that the photons are propagating close to each other and that the pulse width is narrow, the nonlinear term may be approximated by a constant, $B^{\text{T}}(k,x_2-x_1) \approx B^{\text{T}}(k,0)$. Thus we obtain the ideal operation

$$|2\rangle_{\text{out}}^{\text{ideal}} = \left[t_3(k)t_3(k) + B^{\text{T}}(k,0)\right]|2\rangle_{\text{in}}\,, \tag{5.23}$$

which yields the phase shift

$$\theta_2(k) = \arg\left[t_3(k)t_3(k) + B^{\mathrm{T}}(k,0)\right], \tag{5.24}$$

for the two-photon state. The two-photon phase shift with full single-photon transmission, $\theta_2(k_{\mathrm{f}})$, is plotted in Fig. 5.3(a).

5.1.6 Error sources

There are at least three notable error sources for the presented device: finite bandwidth in the photon frequency, the dependence of the nonlinear phase shift on the separation $|x_2 - x_1|$, and the reflection due to the nonlinear interactions between photons.

To study in more detail the errors induced by the finite bandwidth, we note that the transmission coefficient defined by Eq. (5.1) is frequency dependent, and that full transmittance can only be achieved for a single frequency. Assuming a constant qubit transition frequency, for the single-photon transmittance to satisfy $|t_3(k)|^2 \geq 90\%$, we calculate the allowed detuning as a function of the coupling ratio γ. The results are shown in Figs. 5.7(a) and (b). For ratios γ greater than approximatively 0.7, there is no upper limit for the detuning to achieve over 90% transmittance. For large detuning, $\delta \gg \Gamma$, transmittance approaches unity independent of γ. This limit corresponds to the dispersive limit, where the interaction between the photonic field and the qubits is weak.

Another source for errors is the spatial dependency in the two-photon wavefunction. Assuming that the effective pulse width is x_{pulse}, we quantify the error in the two-photon state as

$$\begin{aligned}\mathcal{E} =& 1 - \frac{1}{A}\left|{}_{\mathrm{out}}\langle 2|2\rangle_{\mathrm{out}}^{\mathrm{ideal}}\right| \\ =& 1 - \frac{1}{A}\left|\int_{-x_{\mathrm{pulse}}/2}^{x_{\mathrm{pulse}}/2} dx_1 \int_{-x_{\mathrm{pulse}}/2}^{x_{\mathrm{pulse}}/2} dx_2 \left[t_3(k)t_3(k) + B^{\mathrm{T}}(k, x_2 - x_1)\right]^* \times \right. \\ & \left. \left[t_3(k)t_3(k) + B^{\mathrm{T}}(k,0)\right]\right|,\end{aligned} \tag{5.25}$$

where we normalize the wavefunctions according to the pulse width, such that $A = \sqrt{{}^{\mathrm{ideal}}_{\mathrm{out}}\langle 2|2\rangle_{\mathrm{out}}^{\mathrm{ideal}}\,{}_{\mathrm{out}}\langle 2|2\rangle_{\mathrm{out}}}$, where the integration is carried out over the same interval as in Eq. (5.25). The error in the two-photon state as a function of pulse width is presented in Fig. 5.7(b). The states overlap the most with narrow pulses, hence giving the smallest error. For longer pulses, the amount of overlap is decreased.

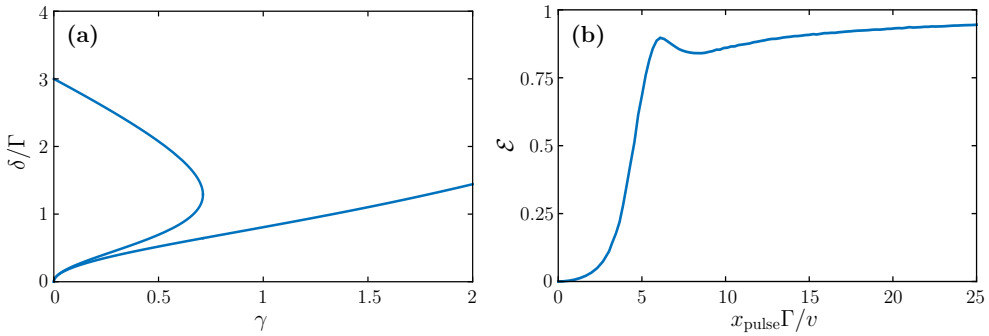

Figure 5.7: (a) Bottom curve corresponds to the lower limit and the top curve to the upper limit of the detuning for the single-photon transmission to satisfy $|t(k)|^2 \geq 90\%$ as a function of coupling ratio γ. (d) The error in the two-photon wavefunction, $\mathcal{E}$, as a function of effective pulse width, x_{pulse}. The coupling ratio is set to correspond to $\pi/4$ nonlinearity in phase, with $\gamma \approx 0.62$

5.2 Two-qubit gates

5.2.1 Conditional-phase-shift gate

In this section, we show how the nonlinear phase shifter device can be used as a component in a conditional-phase-shift (CPS) gate for a microwave photonic quantum computer. A design for such a gate was proposed in Ref. [26], and is presented in Fig. 5.8.

We define the computational two-qubit basis in the dual-rail representation as $\{|00_{\mathrm{Q}}\rangle, |01_{\mathrm{Q}}\rangle, |10_{\mathrm{Q}}\rangle, |11_{\mathrm{Q}}\rangle\}$, where the basis vectors are given by

$$\hat{a}^\dagger_{\mathrm{in}}\hat{d}^\dagger_{\mathrm{in}}|0\rangle = |1001\rangle \equiv |00_{\mathrm{Q}}\rangle, \tag{5.26}$$

$$\hat{a}^\dagger_{\mathrm{in}}\hat{c}^\dagger_{\mathrm{in}}|0\rangle = |1010\rangle \equiv |01_{\mathrm{Q}}\rangle, \tag{5.27}$$

$$\hat{b}^\dagger_{\mathrm{in}}\hat{d}^\dagger_{\mathrm{in}}|0\rangle = |0101\rangle \equiv |10_{\mathrm{Q}}\rangle, \tag{5.28}$$

$$\hat{b}^\dagger_{\mathrm{in}}\hat{c}^\dagger_{\mathrm{in}}|0\rangle = |0110\rangle \equiv |11_{\mathrm{Q}}\rangle, \tag{5.29}$$

where $\hat{a}^\dagger_{\mathrm{in}}$, $\hat{b}^\dagger_{\mathrm{in}}$, $\hat{c}^\dagger_{\mathrm{in}}$, and $\hat{d}^\dagger_{\mathrm{in}}$ act as the creation operators for photons of wavenumber k for each line separately.

Throughout the rest of this section, we assume that the wavenumber of the photons is set to correspond to full single-photon transmission, $k = k_{\mathrm{f}}$. For $|00_{\mathrm{Q}}\rangle$, $|01_{\mathrm{Q}}\rangle$, and $|10_{\mathrm{Q}}\rangle$, the response of the CPS gate can be calculated with the result of Eq. (5.20) and by using the linear scattering equations for the beam splitters and phase shifters [26]. As a result, each of the single-photon states acquire the phase $\theta_1(k_{\mathrm{f}})$ defined by Eq. (5.11). Thus, the qubit

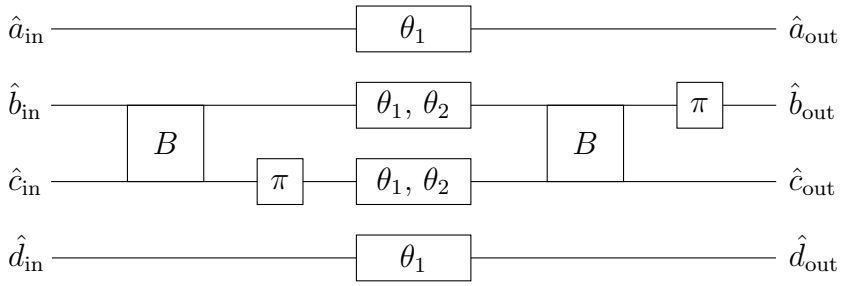

Figure 5.8: Design for the CPS gate as was proposed in Ref. [26]. The gate consists of two 50:50 beam splitters B, two linear phase shifters with a constant phase shift of π radians, two linear phase shifters, and two nonlinear phase shifters. The linear and nonlinear phase shifters act on a single-photon state by shifting the phase by $\theta_1(k)$. In addition, the nonlinear phase shifter shifts the phase of a two-photon state by $\theta_2(k)$.

basis states transform in the CPS gate as

$$|00_{\text{Q}}\rangle \to \hat{a}^\dagger_{\text{out}}\hat{d}^\dagger_{\text{out}}\,|0\rangle = e^{2i\theta_1(k_{\text{f}})}\,|00_{\text{Q}}\rangle\,, \tag{5.30}$$

$$|01_{\text{Q}}\rangle \to \hat{a}^\dagger_{\text{out}}\hat{c}^\dagger_{\text{out}}\,|0\rangle = e^{2i\theta_1(k_{\text{f}})}\,|01_{\text{Q}}\rangle\,, \tag{5.31}$$

$$|10_{\text{Q}}\rangle \to \hat{b}^\dagger_{\text{out}}\hat{d}^\dagger_{\text{out}}\,|0\rangle = e^{2i\theta_1(k_{\text{f}})}\,|10_{\text{Q}}\rangle\,. \tag{5.32}$$

With the input state $|11_{\text{Q}}\rangle$, the response is no longer purely linear. After the first beam splitter, the state is a superposition of two states with two photons propagating in second or third lines due to the Hong–Ou–Mandel effect. These superposition states acquire a phase $\theta_2(k_{\text{f}})$ defined by Eq. (5.24). Hence, the state $|11_{\text{Q}}\rangle$ transform as [26]

$$|11_{\text{Q}}\rangle \to \hat{b}^\dagger_{\text{out}}\hat{c}^\dagger_{\text{out}}\,|0\rangle = e^{i\theta_2(k_{\text{f}})}\,|11_{\text{Q}}\rangle\,. \tag{5.33}$$

In the computational basis described above, the matrix describing the CPS gate is written as

$$U_{\text{CPS}}(k_{\text{f}}) = \begin{pmatrix} e^{2i\theta_1(k_{\text{f}})} & 0 & 0 & 0 \\ 0 & e^{2i\theta_1(k_{\text{f}})} & 0 & 0 \\ 0 & 0 & e^{2i\theta_1(k_{\text{f}})} & 0 \\ 0 & 0 & 0 & e^{i\theta_2(k_{\text{f}})} \end{pmatrix}. \tag{5.34}$$

Neglecting a global phase of $2\theta_1(k_{\text{f}})$, we observe that the $|11_{\text{Q}}\rangle$ component acquires a nonlinear phase shift of $\theta_2(k_{\text{f}}) - 2\theta_1(k_{\text{f}})$. With the nonlinear phase shifter design presented in Sec. 5.1, a nonlinear phase shift between 0 and approximately $3\pi/10$ radians can be generated by tuning the coupling ratio γ [see Fig. 5.3(a)].

5.2.2 Controlled-Z gate

Using the CPS gate described by Eq. (5.34), we may implement a CZ gate in the dual-rail representation. The wavenumbers of the photons are set to $k = k_{\mathrm{f}}$ such that the single-photon states are fully transmitted. The coupling ratio γ can be tuned such that the nonlinear phase shift equals to $\theta_2(k_{\mathrm{f}}) - 2\theta_1(k_{\mathrm{f}}) = \pi/4$ radians. This is obtained with the coupling ratio $\gamma_{\mathrm{CZ}} \approx 0.62$.

We place four nonlinear phase shifters consecutively, instead of one, and as a result obtain the gate operation

$$\begin{aligned} U_{\mathrm{CPS}}(k_{\mathrm{f}})^4 &= \begin{pmatrix} e^{8i\theta_1(k_{\mathrm{f}})} & 0 & 0 & 0 \\ 0 & e^{8i\theta_1(k_{\mathrm{f}})} & 0 & 0 \\ 0 & 0 & e^{8i\theta_1(k_{\mathrm{f}})} & 0 \\ 0 & 0 & 0 & e^{i\pi+8i\theta_1(k_{\mathrm{f}})} \end{pmatrix} \\ &= e^{8i\theta_1(k_{\mathrm{f}})} \begin{pmatrix} 1 & 0 & 0 & 0 \\ 0 & 1 & 0 & 0 \\ 0 & 0 & 1 & 0 \\ 0 & 0 & 0 & -1 \end{pmatrix} \\ &= e^{8i\theta_1(k_{\mathrm{f}})}\mathrm{CZ}. \end{aligned} \tag{5.35}$$

Thus, up to a global phase factor, this scheme corresponds to the CZ gate operation.

5.2.3 Gate fidelities

The fidelity of the quantum gate is estimated as [13]

$$\mathcal{F}_{|\psi\rangle} = \min_{|\psi\rangle} \left| \langle\psi| \hat{U}^{\dagger}_{\mathrm{approx}} \hat{U}_{\mathrm{ideal}} |\psi\rangle \right|, \tag{5.36}$$

where $|\psi\rangle = c_0 |00_{\mathrm{Q}}\rangle + c_1 |01_{\mathrm{Q}}\rangle + c_2 |10_{\mathrm{Q}}\rangle + c_3 |11_{\mathrm{Q}}\rangle$, $\hat{U}_{\mathrm{approx}}$ corresponds to the implemented gate operation, and $\hat{U}_{\mathrm{ideal}}$ to the ideal operation. The state $|\psi\rangle$ is normalized, i.e., we have the restriction $\sum_{i=0}^{3} |c_i|^2 = 1$ in the minimization routine. In the absence of errors, $\hat{U}_{\mathrm{approx}}$ coincides with $\hat{U}_{\mathrm{ideal}}$, and hence the fidelity becomes unity.

First, we calculate the fidelity of the implemented CPS gate (see Sec. 5.2.1).

For ideal operation, we have

$$\hat{U}_{\mathrm{CPS}}^{\mathrm{ideal}} |00_{\mathrm{Q}}\rangle = e^{2i\theta_1(k_{\mathrm{f}})} |00_{\mathrm{Q}}\rangle \,, \tag{5.37}$$

$$\hat{U}_{\mathrm{CPS}}^{\mathrm{ideal}} |01_{\mathrm{Q}}\rangle = e^{2i\theta_1(k_{\mathrm{f}})} |01_{\mathrm{Q}}\rangle \,, \tag{5.38}$$

$$\hat{U}_{\mathrm{CPS}}^{\mathrm{ideal}} |10_{\mathrm{Q}}\rangle = e^{2i\theta_1(k_{\mathrm{f}})} |10_{\mathrm{Q}}\rangle \,, \tag{5.39}$$

$$\hat{U}_{\mathrm{CPS}}^{\mathrm{ideal}} |11_{\mathrm{Q}}\rangle = e^{i\theta_2(k_{\mathrm{f}})} |11_{\mathrm{Q}}\rangle \,. \tag{5.40}$$

We assume that the nonlinear phase shifters are the dominating source of error. The errors in the $|00_{\mathrm{Q}}\rangle$ component are thus assumed negligible, since the photons in this case pass only through linear phase shifters (see Fig. 5.8).

In the case of $|10_{\mathrm{Q}}\rangle$ and $|01_{\mathrm{Q}}\rangle$ states, one single-photon state propagates through the nonlinear phase shifter and the another single-photon state through the linear phase shifter. For these states, we make the assumption that a single nonlinear phase shifter device introduces an error of $\Delta\theta_1$ in the phase of the photon propagating through it. Consequently, we may write

$$\hat{U}_{\mathrm{CPS}}^{\mathrm{approx}} |00_{\mathrm{Q}}\rangle = e^{2i\theta_1(k_{\mathrm{f}})} |00_{\mathrm{Q}}\rangle \,, \tag{5.41}$$

$$\hat{U}_{\mathrm{CPS}}^{\mathrm{approx}} |01_{\mathrm{Q}}\rangle = e^{i[2\theta_1(k_{\mathrm{f}})+\Delta\theta_1]} |01_{\mathrm{Q}}\rangle \,, \tag{5.42}$$

$$\hat{U}_{\mathrm{CPS}}^{\mathrm{approx}} |10_{\mathrm{Q}}\rangle = e^{i[2\theta_1(k_{\mathrm{f}})+\Delta\theta_1]} |10_{\mathrm{Q}}\rangle \,. \tag{5.43}$$

With the input state $|11_{\mathrm{Q}}\rangle$, two photons propagate through the nonlinear phase shifter simultaneously. The operation of $\hat{U}_{\mathrm{CPS}}^{\mathrm{approx}}$ on the state $|11_{\mathrm{Q}}\rangle$ is rewritten as

$$\begin{aligned}
\hat{U}_{\mathrm{CPS}}^{\mathrm{approx}} |11_{\mathrm{Q}}\rangle &= \hat{A}\hat{U}_{\mathrm{NL}}\hat{B} |11_{\mathrm{Q}}\rangle \\
&= \hat{A}\hat{U}_{\mathrm{NL}} \frac{1}{\sqrt{2}} \left(|20\rangle_{\mathrm{in}} - |02\rangle_{\mathrm{in}} \right) \\
&= \hat{A} \frac{1}{\sqrt{2}} \left(|20\rangle_{\mathrm{out}} - |02\rangle_{\mathrm{out}} \right) ,
\end{aligned}$$

where $\hat{A}$ and $\hat{B}$ are the operations introduced by the beam splitters and constant phase shifters after and before the nonlinear phase shifter, respectively, and $\hat{U}_{\mathrm{NL}}$ is the operation of the nonlinear phase shifters. The states $|20\rangle_{\mathrm{in}}$ and $|02\rangle_{\mathrm{in}}$ are the two-photon input states, in which two photons propagate on second and third lines [see Eq. (5.21)]. The nonlinear phase shifters transform these states to $|20\rangle_{\mathrm{out}}$ and $|02\rangle_{\mathrm{out}}$, respectively. The fidelity of the CPS

gate can be expressed as

$$\begin{aligned}
\mathcal{F}_{|\psi\rangle} =& \min_{|\psi\rangle} \left| \langle\psi| \left(\hat{U}_{\mathrm{CPS}}^{\mathrm{approx}}\right)^{\dagger} \hat{U}_{\mathrm{CPS}}^{\mathrm{ideal}} |\psi\rangle \right| = \min_{|\psi\rangle} \left| \left(\hat{U}_{\mathrm{CPS}}^{\mathrm{approx}} |\psi\rangle\right)^{\dagger} \hat{U}_{\mathrm{CPS}}^{\mathrm{ideal}} |\psi\rangle \right| \\
=& \min_{|\psi\rangle} \Big| \Big[c_1 e^{2i\theta_1(k_{\mathrm{f}})} |00_{\mathrm{Q}}\rangle + c_2 e^{i[2\theta_1(k_{\mathrm{f}})+\Delta\theta_1]} |01_{\mathrm{Q}}\rangle + c_3 e^{i[2\theta_1(k_{\mathrm{f}})+\Delta\theta_1]} |10_{\mathrm{Q}}\rangle \\
& + c_4 \hat{A} \frac{1}{\sqrt{2}} \left(|20\rangle_{\mathrm{out}} - |02\rangle_{\mathrm{out}} \right) \Big]^{\dagger} \Big[c_1 e^{2i\theta_1(k_{\mathrm{f}})} |00_{\mathrm{Q}}\rangle + c_2 e^{2i\theta_1(k_{\mathrm{f}})} |01_{\mathrm{Q}}\rangle \\
& + c_3 e^{2i\theta_1(k_{\mathrm{f}})} |10_{\mathrm{Q}}\rangle + c_4 \hat{A} \frac{1}{\sqrt{2}} \left(|20\rangle_{\mathrm{out}}^{\mathrm{ideal}} - |02\rangle_{\mathrm{out}}^{\mathrm{ideal}} \right) \Big] \Big| \\
=& \min_{|\psi\rangle} \Big| |c_1|^2 + |c_2|^2 e^{-i\Delta\theta_1} + |c_3|^2 e^{-i\Delta\theta_1} \\
& + |c_4|^2 \frac{1}{2} \left({}_{\mathrm{out}}\langle 20|20\rangle_{\mathrm{out}}^{\mathrm{ideal}} + {}_{\mathrm{out}}\langle 02|02\rangle_{\mathrm{out}}^{\mathrm{ideal}} \right) \Big|, \qquad (5.44)
\end{aligned}$$

where we have used the facts that the qubit basis states are orthogonal to each other and $\hat{A}$ is a unitary transformation. Furthermore, the operations of the nonlinear phase shifters on the two-photon states are assumed identical. Hence, the two-photon output states, $|20\rangle_{\mathrm{out}}$ and $|02\rangle_{\mathrm{out}}$, are both defined as in Eq. (5.22). The ideal output states are defined by Eq. (5.23).

We approximate the maximum error in the linear cases, $\Delta\theta_{1,\mathrm{max}}$, by first assuming an uncertainty $\Delta\delta$ in the detuning between the frequencies of the photon and the qubit. Keeping the coupling ratio fixed at $\gamma_{\mathrm{CZ}} \approx 0.62$, and the wavenumber at $k = k_{\mathrm{f}}$, we estimate $\Delta\theta_{1,\mathrm{max}}$ by calculating the difference in the argument of the transmission coefficient defined by Eq. (5.1) with the detunings set to δ_{f} and $\delta_{\mathrm{f}} \pm \Delta\delta/2$. In the minimization routine, we let $|\Delta\theta_1| \leq \Delta\theta_{1,\mathrm{max}}$. In the two-photon case, the overlap between the calculated and the ideal output states is calculated as in Eq. (5.25).

The spatial length of the pulse is related to the temporal pulse width as $x_{\mathrm{pulse}} = v t_{\mathrm{pulse}}$, where $v \approx 10^8$ m/s. Assuming a bandwidth equivalent to $\Delta\delta$ in the photon frequency, we allow the minimum pulse duration $t_{\mathrm{pulse}} = 2\pi/\Delta\delta$. In the calculation of the fidelity, we optimize the pulse duration to maximize fidelity.

Within these approximations, we obtain the CPS gate fidelity $\mathcal{F}_{|\psi\rangle} \approx 0.35$ with $t_{\mathrm{pulse}} \approx 0.8$ μs and $\Delta\delta \approx 2\pi \times 1.25$ MHz. With short pulse widths, the approximated error $\Delta\theta_1$ dominates, and with longer pulses, the error introduced by the two-photon state starts to dominate. As examples, for a shorter pulse ($t_{\mathrm{pulse}} \approx 0.7$ μs and $\Delta\delta \approx 2\pi \times 1.4$ MHz), we have $\mathcal{F}_{|\psi\rangle} \approx 0.21$, and for a longer pulse ($t_{\mathrm{pulse}} \approx 0.9$ μs and $\Delta\delta \approx 2\pi \times 1.1$ MHz), we have $\mathcal{F}_{|\psi\rangle} \approx 0.10$.

We find that the value of the decay rate does not play an important part

in this error analysis. In the above calculations, we have assumed the qubit decay rate $\Gamma = 2\pi$ MHz, which is an experimentally reasonable value. By choosing a slower decay rate, we could allow longer pulses without affecting the error. However, the photon bandwidth would also have to be narrower. With faster decay rate, the situation is opposite.

The implemented CZ gate contains four nonlinear phase shifters placed adjacently. Assuming that the nonlinear phase shifters act identically on the transmitted two-photon states, we may estimate the fidelity of the CZ gate roughly as $\left(\mathcal{F}_{|\psi\rangle}\right)^4 \approx 0.02$, where $\mathcal{F}_{|\psi\rangle}$ is the fidelity of the CPS gate with one nonlinear phase shifter.

Chapter 6

Conclusions

In this thesis, we studied the properties of microwave photons as they propagate in a superconducting transmission line to which multiple superconducting qubits are coupled. More precisely, the scattering of the propagating one- and two-photon input states from the qubits was theoretically investigated. The results of this thesis can potentially be used in the implementation of a microwave photon based quantum computer or other quantum devices that make use of microwave photons propagating in superconducting circuits.

Starting from the distributed-element model, we reviewed in detail the quantization procedure for the transmission line to which multiple superconducting qubits are capacitively coupled. Furthermore, we reviewed the formalism of a recently published technique, presented in Ref. [29], for calculating the effective interactions between two photons propagating in the transmission line to which multiple qubits are coupled.

We presented a design for a nonlinear phase shifter device for microwave photons in superconducting circuits. The proposed design utilizes the strong coupling between the superconducting qubits and the microwave field, giving rise to effective interactions between the photons. The linear and nonlinear responses of the system with one- and two-photon input states were analyzed using the reviewed methods. In addition, we showed how entangling two-qubit gates can be implemented with the presented nonlinear phase shifter device. The possible error sources in the nonlinear phase shifter lowering the quantum gate fidelity were also identified.

The studied nonlinear phase shifter constitutes a minimal implementation of a symmetric system where two photons effectively interact with each other through excitations of more than one superconducting qubit. The amount of nonlinear phase shift induced by a single device can potentially be enhanced by adding more qubits to the system. Furthermore, the transition frequencies of the qubits were kept uniform in our analysis. Allowing the qubits to have

different transition frequencies can possibly be used to further increase the nonlinear response of the system.

The results of this thesis indicate that superconducting qubits can be used to induce effective interactions between microwave photons in a way that they can ultimately be used in the implementation of entangling two-qubit quantum gates. However, the fidelities of the presented quantum gates are rather low. One way to improve the fidelities could be optimizing the parameters of the system, such as the number of superconducting qubits coupled to the transmission line. Furthermore, considering more realistic wavepackets instead of plane waves, for example through numerical simulations, is an interesting future research avenue.

References

[1] R. P. Feynman, Int. J. Theor. Phys. **21**, 467 (1982).

[2] D. Deutsch, Proc. R. Soc. London, Ser. A **400**, 97 (1985).

[3] P. Shor, in *Proc. 35th Annual Symposium on Foundations of Computer Science,* edited by S. Goldwasser (IEEE Computer Society Press, Los Alamitos, 1994) pp. 124–134.

[4] L. K. Grover, Phys. Rev. Lett. **79**, 325 (1997).

[5] C. Monroe, D. M. Meekhof, B. E. King, W. M. Itano, and D. J. Wineland, Phys. Rev. Lett. **75**, 4714 (1995).

[6] D. G. Cory, A. F. Fahmy, and T. F. Havel, Proc. Natl. Acad. Sci. U.S.A. **94**, 1634 (1997).

[7] B. E. Kane, Nature **393**, 133 (1998).

[8] D. Loss and D. P. DiVincenzo, Phys. Rev. A **57**, 120 (1998).

[9] E. Knill, R. Laflamme, and G. J. Milburn, Nature **409**, 46 (2000).

[10] A. Blais, R.-S. Huang, A. Wallraff, S. M. Girvin, and R. J. Schoelkopf, Phys. Rev. A **69**, 062320 (2004).

[11] J. Volz, M. Scheucher, C. Junge, and A. Rauschenbeutel, Nature Photon. **8**, 965 (2014).

[12] M. Hua, M.-J. Tao, and F.-G. Deng, Phys. Rev. A **90**, 012328 (2014).

[13] M. A. Nielsen and I. L. Chuang, *Quantum Computation and Quantum Information* (Cambridge University Press, Cambridge, 2000).

[14] A. Barenco, C. H. Bennett, R. Cleve, D. P. DiVincenzo, N. Margolus, P. Shor, T. Sleator, J. A. Smolin, and H. Weinfurter, Phys. Rev. A **52**, 3457 (1995).

[15] C. K. Hong, Z. Y. Ou, and L. Mandel, Phys. Rev. Lett. **59**, 2044 (1987).

[16] L. N. Cooper, Phys. Rev. **104**, 1189 (1956).

[17] J. Bardeen, L. N. Cooper, and J. R. Schrieffer, Phys. Rev. **108**, 1175 (1957).

[18] V. Bouchiat, D. Vion, P. Joyez, D. Esteve, and M. H. Devoret, Phys. Scripta **1998**, 165 (1998).

[19] J. Koch, T. M. Yu, J. Gambetta, A. A. Houck, D. I. Schuster, J. Majer, A. Blais, M. H. Devoret, S. M. Girvin, and R. J. Schoelkopf, Phys. Rev. A **76**, 042319 (2007).

[20] D. Walls and G. Milburn, *Quantum Optics* (Springer-Verlag, Berlin, 1994).

[21] P. Lambropoulos and D. Petrosyan, *Fundamentals of Quantum Optics and Quantum Information* (Springer-Verlag Berling, Heidelberg, 2007).

[22] H. Jin-Song, L. Yan-Ling, and W. Lian-Fu, Commun. Theor. Phys. **60**, 601 (2013).

[23] K. Lalumière, B. C. Sanders, A. F. van Loo, A. Fedorov, A. Wallraff, and A. Blais, Phys. Rev. A **88**, 043806 (2013).

[24] M. Devoret, in *Quantum Fluctuations in Electrical Circuits,* edited by S. Reynaud, E. Giacobino, and J. Zinn-Justin (Elsevier Science, New York, 1997).

[25] B. Peropadre, J. Lindkvist, I.-C. Hoi, C. M. Wilson, J. J. Garcia-Ripoll, P. Delsing, and G. Johansson, New J. Phys. **15**, 035009 (2013).

[26] J. Kokkala, Master's thesis, Aalto University, 2013.

[27] H. Zheng, Ph.D. thesis, Duke University, 2013.

[28] J.-T. Shen and S. Fan, Phys. Rev. Lett. **95**, 213001 (2005).

[29] H. Zheng and H. U. Baranger, Phys. Rev. Lett. **110**, 113601 (2013).

[30] J.-T. Shen and S. Fan, Phys. Rev. A **79**, 023837 (2009).

[31] J.-T. Shen and S. Fan, Phys. Rev. A **76**, 062709 (2007).

[32] H. Zheng, D. J. Gauthier, and H. U. Baranger, Phys. Rev. A **82**, 063816 (2010).

[33] J. J. Sakurai, *Modern Quantum Mechanics* (Addison-Wesley, Reading, MA, 1994).

[34] A. Dhar, D. Sen, and D. Roy, Phys. Rev. Lett. **101**, 066805 (2008).

[35] J. H. Mathews and R. W. Howell, *Complex Analysis for Mathematics and Engineering* (Jones and Bartlett Publishers, Massachusetts, 2006).

[36] X.-W. Xu and Y. Li, Phys. Rev. A **90**, 033832 (2014).

Appendix A

Single-photon scattering coefficients

In this appendix, we calculate the coefficients of the eigenstate of Eq. (4.1) related to single-photon scattering from a single two-level system. First, we take the Hamiltonian of Eq. (3.60), and write the Schrödinger equation $\hat{\mathcal{H}}\left|\phi_1(k);\alpha\right\rangle = E\left|\phi_1(k);\alpha\right\rangle$ for both cases $\alpha = \mathrm{R}, \mathrm{L}$ separately. The Schrödinger equation provides us with

$$\left(-i\hbar v\frac{d}{dx} - E\right)\phi_{\mathrm{R}}^{\mathrm{R}}(k,x) + \hbar g\delta(x)e^{\mathrm{R}}(k) = 0, \tag{A.1}$$

$$\left(i\hbar v\frac{d}{dx} - E\right)\phi_{\mathrm{L}}^{\mathrm{R}}(k,x) + \hbar g\delta(x)e^{\mathrm{R}}(k) = 0, \tag{A.2}$$

$$(\hbar\Omega - E)e^{\mathrm{R}}(k) + \hbar g\left[\phi_{\mathrm{R}}^{\mathrm{R}}(k,0) + \phi_{\mathrm{L}}^{\mathrm{R}}(k,0)\right] = 0, \tag{A.3}$$

$$\left(-i\hbar v\frac{d}{dx} - E\right)\phi_{\mathrm{R}}^{\mathrm{L}}(k,x) + \hbar g\delta(x)e^{\mathrm{L}}(k) = 0, \tag{A.4}$$

$$\left(i\hbar v\frac{d}{dx} - E\right)\phi_{\mathrm{L}}^{\mathrm{L}}(k,x) + \hbar g\delta(x)e^{\mathrm{L}}(k) = 0, \tag{A.5}$$

$$(\hbar\Omega - E)e^{\mathrm{L}}(k) + \hbar g\left[\phi_{\mathrm{R}}^{\mathrm{L}}(k,0) + \phi_{\mathrm{L}}^{\mathrm{L}}(k,0)\right] = 0. \tag{A.6}$$

We proceed by inserting the wavefunctions of Eqs. (4.2)–(4.5) into Eqs. (A.1)–(A.6). For the equations containing the Dirac delta function, we integrate and take the limit as $\lim_{\epsilon\to 0}\int_{-\epsilon}^{\epsilon} dx$. In the case of multiple qubits coupled to the waveguide, this integral is taken over all of the qubit sites separately as $\lim_{\epsilon\to 0}\int_{x_i-\epsilon}^{x_i+\epsilon} dx$, where x_i denotes the location of the ith qubit site. Furthermore, we note that the energy is given by $E = \hbar v k$. Following these steps,

we arrive at

$$-\frac{i\hbar v}{\sqrt{2\pi}}\left[-1+t_1^{\mathrm{R}}(k)\right]+\hbar g e^{\mathrm{R}}(k)=0 \tag{A.7}$$

$$\frac{i\hbar v}{\sqrt{2\pi}}\left[-r_1^{\mathrm{R}}(k)\right]+\hbar g e^{\mathrm{R}}(k)=0 \tag{A.8}$$

$$(\hbar\Omega-\hbar vk)e^{\mathrm{R}}(k)+\hbar g\left\{\frac{1}{2\sqrt{2\pi}}\left[1+t_1^{\mathrm{R}}(k)+r_1^{\mathrm{R}}(k)\right]\right\}=0, \tag{A.9}$$

$$-\frac{i\hbar v}{\sqrt{2\pi}}\left[r_1^{\mathrm{L}}(k)\right]+\hbar g e^{\mathrm{L}}(k)=0 \tag{A.10}$$

$$\frac{i\hbar v}{\sqrt{2\pi}}\left[-t_1^{\mathrm{L}}(k)+1\right]+\hbar g e^{\mathrm{L}}(k)=0 \tag{A.11}$$

$$(\hbar\Omega-\hbar vk)e^{\mathrm{L}}(k)+\hbar g\left\{\frac{1}{2\sqrt{2\pi}}\left[r_1^{\mathrm{L}}(k)+t_1^{\mathrm{L}}(k)+1\right]\right\}=0, \tag{A.12}$$

By solving this system of equations, we find the following solutions for the scattering coefficients

$$t_1^R(k)=t_1^L(k)=\frac{1}{1+i\Gamma/\left[\sqrt{2\pi}(2vk-2\Omega)\right]}, \tag{A.13}$$

$$r_1^R(k)=r_1^L(k)=-\frac{\Gamma}{\Gamma-2i\sqrt{2\pi}(vk-\Omega)}, \tag{A.14}$$

$$e_1^R(k)=e_1^L(k)=-\frac{i\sqrt{2v\Gamma}}{\Gamma-2i\sqrt{2\pi}(vk-\Omega)}, \tag{A.15}$$

where we have defined the decay rate as [29]

$$\Gamma=2g^2/v=4\pi V^2. \tag{A.16}$$

In the case of multiple qubits, the derivation of the scattering coefficients is carried out with identical steps a above.

Appendix B

Nonlinear corrections

In this appendix, we give the exact forms of the nonlinear correction terms appearing in the transmitted and reflected two-photon wavefunctions for $x_1 = x_2$. The correction term for the transmitted two-photon wavefunction [see Eq. (5.14)] reads

$$B^{\mathrm{T}}(k,0) = \frac{f^{\mathrm{T}}}{g^{\mathrm{T}}}, \tag{B.1}$$

where we have defined the functions

$$\begin{aligned} f^{\mathrm{T}} =& \Gamma^9\left[-(\gamma-2)\right]\gamma^3 + 3i\Gamma^8\delta(\gamma-2)\gamma^3 + \Gamma^7\delta^2\gamma^2\left[\gamma(2\gamma-5)-10\right] \\ &+ 2i\Gamma^6\delta^3\gamma^2\left[\gamma(\gamma+4)+18\right]\left(\gamma^2+2\right) + \Gamma^5\delta^4\gamma\left\{\gamma\left[\gamma(3\gamma+23)\right.\right. \\ &\left.\left.+60\right]+20\right\} - i\Gamma^4\delta^5\gamma\left\{\gamma\left[\gamma(\gamma+24)+66\right]+60\right\} \\ &- 8\Gamma^3\delta^6\left\{\gamma\left[\gamma(\gamma+6)+6\right]+2\right\} + 16i\Gamma^2\delta^7, \end{aligned} \tag{B.2}$$

$$\begin{aligned} g^{\mathrm{T}} =& (\Gamma - i\delta)^2[\Gamma(\gamma+2) - 4i\delta]\left[-4\delta^2 + \Gamma^2\gamma - i\Gamma\delta(\gamma+2)\right]\times \\ &\left[-2\delta^2 + \Gamma\gamma(\Gamma - i\delta)\right]^2. \end{aligned} \tag{B.3}$$

For the reflected two-photon wavefunction [see Eq. (5.15)], we have

$$B^{\mathrm{R}}(k,0) = \frac{f^{\mathrm{R}}}{g^{\mathrm{R}}}, \tag{B.4}$$

with the definitions

$$\begin{aligned} f^{\mathrm{R}} =& \Gamma^9\gamma^3(3\gamma+2) - i\Gamma^8\delta\gamma^3(9\gamma+14) - 5\Gamma^7\delta^2\gamma^2\left[\gamma(2\gamma+9)+2\right] \\ &+2i\Gamma^6\delta^3\gamma^2\left[\gamma(3\gamma+32)+26\right] + \Gamma^5\delta^4\gamma\left\{\gamma\left[\gamma(3\gamma+47)\right.\right. \\ &\left.\left.+108\right]+20\right\} - i\Gamma^4\delta^5\gamma\left\{\gamma\left[\gamma(\gamma+24)+98\right]+60\right\} \\ &- 8\Gamma^3\delta^6\left\{\gamma\left[\gamma(\gamma+6)+6\right]+2\right\} + 16i\Gamma^2\delta^7\left(\gamma^2+2\right), \end{aligned} \tag{B.5}$$

$$\begin{aligned} g^{\mathrm{R}} =& (\Gamma - i\delta)^2[\Gamma(\gamma+2) - 4i\delta]\left[-4\delta^2 + \Gamma^2\gamma - i\Gamma\delta(\gamma+2)\right]\times \\ &\left[-2\delta^2 + \Gamma\gamma(\Gamma - i\delta)\right]^2. \end{aligned} \tag{B.6}$$